https://doi.org/10.1016/j.surfcoat.2020.126804

Enhancement in corrosion and electrical wear resistance of copper via laser surface alloying with NiTi

C.T. Kwok[a,b], P.K. Wong[a], H.C. Man[c]

[a] Department of Electromechanical Engineering, University of Macau, China

[b] Institute of Applied Physics and Materials Engineering, University of Macau, China

[c] Department of Industrial and Systems Engineering, The Hong Kong Polytechnic University, Hong Kong, China

Abstract

With a 2.3-kW high-power diode laser, laser surface alloying of a commercially pure copper (cp Cu) with NiTi powder was carried out to attain higher corrosion and electrical wear resistances. Potentiodynamic polarization was conducted in simulated acid rain (SAR) at 25 ^{o}C for simulating the corrosive environment. In the SAR, corrosion potentials of all laser-alloyed samples are found to be nobler than those of cp Cu and NiTi alloy and their corrosion current densities are lower than that of cp Cu although their oxide layers are less uniform. Electrical wear tests were also carried out in both dry and wet conditions with a pin-on-disc tribometer. The electrical wear resistances of the laser-alloyed samples in wet condition are higher than in dry condition due to lubrication effect and reduction in frictional heat. The electrical wear resistances of all laser-alloyed samples were improved as compared with cp Cu owing to the presence of pseudo-plasticity of B19' and hard IMPs, and work hardening effect during electrical wear. The contribution of electrical wear in SAR is mainly mechanical wear, and wear-corrosion synergism up to 36.1%, while corrosion is negligible. Compared with cp Cu, the interfacial contact resistance of the laser-alloyed

samples at 50 N/cm^2 has increased from 3.5 to 7.2 times.

Keywords: Laser surface alloying, NiTi, copper, corrosion, electrical sliding wear

1. Introduction

Copper is widely applied in electric contacts due to its high thermal and electrical conductivities. It also possesses high ductility, good machinability, and affordable price [1]. However, its drawbacks include low hardness, and being susceptible to wear and corrosion in harsh environments. For instance, contact wires of the overhead traction system and current collector shoes of the third-rail system are mainly made of copper and its alloys for supplying electrical energy to the locomotives. The performance of an electric contact system depends on the electrical and mechanical properties of the contact materials and working conditions including contact force, moving speed, electric current and environmental conditions, including fog, acid rain and snow [2-4]. Particularly, sliding friction in the presence of electric current can further increases the temperature of the surface by Joule heating and arc discharge, and hence increases the wear rate [5-8]. In some circumstances, the surface of the contact materials will be worn with the presence of acid rain. To improve the hardness, wear and corrosion resistances, fabrication of a protective surface coating on cp Cu is desirable while its desirable bulk properties are preserved.

Nickel-titanium (NiTi) alloys are extensively applied in tribological and medical applications owing to its superior properties such as superelasticity, shape memory effect, corrosion resistance and biocompatibility [9-17]. Their corrosion resistances are comparable to those of the stainless steels. Their sliding wear and corrosion-erosion resistances are higher than traditional tribo-materials, including steels, Co-based and Ni-based alloys [9-14]. However, NiTi SMA is quite expensive

and thus many efforts have been devoted in developing NiTi coatings using various surfacing techniques including sputtering, plasma spraying, explosive welding, plasma ion plating, laser surfacing and tungsten inert gas surfacing [14, 18-27]. Hiraga and his co-workers fabricated NiTi coatings on titanium alloy Ti6Al4V via laser plasma hybrid spraying [23]. The erosion resistance was reported to be about forty times that of Ti6Al4V. On the other hand, NiTi cladding on austenitic stainless steel 316L was successfully fabricated by laser surfacing and tungsten inert gas surfacing [14, 24-27]. The cavitation erosion was found to be much higher than the 316L substrate. By partially substituting Ni with Cu in the NiTi alloys, a ternary NiTiCu alloy can positively affect many properties such as reducing the characteristic temperatures, hysteresis and dependence on the transformation temperatures [28-31]. Callisti et al. [32] reported that addition of 20-at.% Cu in the NiTi thin films via plasma assisted magnetron sputtering was capable of forming fine and densely dispersed precipitate of $Ti(Ni,Cu)_2$ leading to increase in hardness and elastic modulus. Moreover, Pan et al. reported that adding 5-at.% of Cu in NiTi alloy was able to enhance its corrosion resistance [28]. Also, the ternary alloy NiTiCu with 5 at.% Cu possessed a thicker protective oxide layer when compared to other NiTiCu ternary alloys with 15 at.% and 25 at.% of Cu and NiTi binary alloys [28]. According to the XRD and SEM analyses done by Tatar and his co-workers [33], the major phase in the $Ni_{50-x}Ti_{50}Cu_x$ (x = 14, 17, 20 in at.%) SMAs was found to be martensite (B19) and there was some austenite (B2) as the minor phase. Moreover, $Ti_2(Ni,Cu)$ is a secondary phase which existed in all NiTiCu SMAs. Among the SMAs, the amount of austenite (B2) in $Ni_{36}Ti_{50}Cu_{14}$ was the lowest since M_f is higher than the room temperature. It was also reported that more austenite (B2) was present in the NiTiCu alloys with a higher Cu content.

Laser surfacing of Cu is very challenging owing to its high thermal conductivity and reflectivity to infra-red laser. In particular, only a few studies on laser surface alloying (LSA) of Cu can be found in the literature. LSA of Cu with Cr using CO_2 laser has been reported to improve the wear resistance and hardness without largely sacrificing its electrical conductivity [34-36]. In the previous studies of the present authors, LSA of cp Cu with preplaced Ti powder [37,38] and W powder [39,40] were attempted and the corrosion and electrical wear resistances of the laser-alloyed coatings were found to be higher than that of cp Cu. The corrosion rate of the laser-alloyed cp Cu with Ti and W in 3.5 wt.% NaCl solution was reduced by approximately 15 and 215 times respectively as compared with cp Cu. The enhancement in corrosion resistance was attributed to the existence of Ti or W for forming a more protective oxide layer. On the other hand, their electrical wear resistances were improved by 3 orders of magnitude as compared with cp Cu due to the presence of hard intermetallic phases and W phases [37-40]. However, the interfacial contact resistance (ICR) of the laser-alloyed samples increased with the W or Ti contents and ought to be compromised [39-40]. In the present study, LSA of cp Cu with NiTi was conducted with a high-power diode laser (HPDL) for fabricating novel laser-alloyed NiTiCu layers and their corrosion and electrical sliding wear characteristics and ICR were investigated.

2. Experimental details

2.1 Sample fabrication

cp Cu plates with size of 20 x 20 x 6.3 mm^3 were selected for LSA. NiTi powder with nominal composition of Ni 50 at.% - Ti 50 at.% (Shanghai Xinglu Chemical Technology Co. Ltd., China) and average particle size of 10 μm was used. The cp Cu plates were ground with 80-grit SiC paper in order to increase the surface

roughness for better powder adhesion and for removal of surface oxide. Then the ground plates were cleaned with ethanol and then deionized water before powder preplacement. Polyvinyl alcohol (PVA, 4 wt.%) was used as a binder and was mixed with the NiTi powder to form a slurry. The cp Cu plate was put in the fixture as shown in Fig. 1a. The slurry of NiTi powder was then adhered onto the surface of cp Cu plate using a painting brush or scraper. The sample with the slurry was then dried using a heating fan for 10 minutes. The thickness of the sample was measured using a micrometer screw gauge for controlling the thickness of the slurry to be about 0.15 mm. If the thickness of was more than 0.15 mm, then the sample would be gradually ground using a 1000-grit emery paper until its thickness reached 0.15 mm. Powder preplacement was employed instead of feeding of the powder with an off-axis nozzle to avoid the high reflectivity of cp Cu, to improve the absorptivity of laser energy and to save the precious NiTi powder [35, 36, 41, 42]. The samples were then preheated to 200 ^{o}C with a heating plate to reduce residual stress [44]. LSA was implemented using a 2.3-kW CW HPDL module (Laserline, LDM 1000-1000) with a beam size of 2 mm at a power of 2 kW and scanning speeds of 25, 35 and 45 mm/s. The shorter wavelength of HPDL (990 nm) permitted higher absorptivity for the metals or alloys. The absorptivity of Cu, Ni and Ti at the wavelength of 990 nm are about 9%, 30% and 65% respectively [43]. To avoid oxidation, Argon was applied during LSA as the shielding gas at a flow rate of 15 L/min with a side nozzle. Surfacing was completed by irradiating successive parallel melt tracks with an overlapping ratio of 50%. To reduce the degree of dilution of Cu into the laser-alloyed layer, a second or even third NiTi layer with the same thickness of 0.15 mm was preplaced on the top of the previously laser-alloyed layer and subsequently irradiated by the laser beam again. The dilution ratio (*DR*), which reflects the degree of dilution of alloying elements in the coating, is defined as follows:

$$DR = \left(1 - \frac{t}{D}\right) \times 100\,\% \qquad (1)$$

where t is the preplaced coating thickness (for the samples with two layers, the coating thickness is $2t$, while for coatings with three layers, the coating thickness is $3t$) and D is thickness of the alloyed layers. The processing parameters, including the power, spot size, scanning speeds (25 to 45 mm/s) of the laser beam for the different coatings, and DR are listed in Table 1.

2.2 Microstructural analysis

A scanning-electron microscope (SEM, Hitachi S-3400N) equipped with an energy dispersive X-ray spectrometer (EDS, Horiba EX-250) was used for microstructural and compositional analyses on the cross-section of the laser-alloyed samples. The phases of the samples were determined using a X-ray diffractometer (XRD, Rigaku MiniFlex 600) with *CuK*α radiation operated at 40 kV, 15 mA and a scanning rate of 0.1 °/s. The XRD patterns of the surface of the laser-alloyed samples before and after corrosion and electrical sliding wear tests were also obtained. Moreover, the dislocations in the laser-alloyed samples were examined using the transmission-electron microscopy (TEM, Jeol JEM 2010F). The TEM samples were taken from the center of the top surface of the laser-alloyed Cu samples. The slices with thickness of 1 μm for TEM study were prepared by a SEM equipped with a focused ion beam system (SEM-FIB, Crossbeam, 540 Zeiss).

2.3 Hardness and nanoindentation measurements

Hardness along the depth of cross-section of the laser-alloyed samples was measured using a micro-hardness tester with a load of 200 g and a dwelling duration of 10 s. 5 different locations were chosen for hardness measurement and the average

hardness values were then calculated.

In addition, nanoindentation test was performed on the sample surface using a nanoindenter (Nanomechanics iNano Nanoindenter) at 25 ^{o}C, with a Berkovich diamond indenter and a maximum load F of 50 mN. The surface elastic behavior was characterized by energy recovery ratio (η_w) [25]:

$$\eta_w = \frac{We}{Wt} = \frac{\int_{h_r}^{h_{max}} F\,dh}{\int_{0}^{h_{max}} F\,dh} \quad (2)$$

where W_t and W_e are the total work done and the reversible work done respectively. H_r and h_{max} are the residual depth after unloading and the maximum penetration depth, respectively. A large η_w value reflects good elastic property in indentation.

2.4 Interfacial contact resistance measurement

For measuring the interfacial contact resistance (*ICR*), all samples were machined to a square plate with a surface area of 10 × 10 mm^2. A compression load of 15 to 120 N/cm^2 was applied by a motorized force tester (LTCM-500, Chatillon). The electrical resistance was measured by connecting two cp Cu plates with a DC ohmmeter [45] with an accuracy of ±1 μΩ (GOM-802, Gwinstek) as shown in Fig. 1b. The total measured resistance is the sum of two interfacial components. For cp Cu without the laser-alloyed layer, the two interfacial components are the same, that is two cp Cu / cp Cu plate interfaces ($2R_{Cu/Cu}$); whereas for the laser-alloyed samples, the interfacial components consisted of cp Cu (substrate) / cp Cu plate interface ($R_{Cu/Cu}$) and a laser-alloyed layer / cp Cu plate interface (R_c). The *ICR* of the laser-alloyed layer / Cu plate interface is shown in equation (3).

$$R_c = R_m - R_{Cu/Cu} \quad (3)$$

where R_c = *ICR* of the laser-alloyed layer / cp Cu plate interface; R_m = measured resistance by the ohmmeter; $R_{Cu/Cu}$ = *ICR* of cp Cu / cp Cu plate interface, which is a

constant at a fixed compression load.

2.4 Electrochemical measurements

Rectangular plates of cp Cu and NiTi (for comparison purpose) and the laser-alloyed samples with a surface area of 15 × 15 mm^2 were ground with 800-grit emery paper and then embedded in hot-mount resin. To avoid crevice corrosion, epoxy was applied at the gap between the sample and the mount. The samples with an exposing area of 1 cm^2 were then cleaned and degreased before electrochemical tests. Open-circuit potential (*OCP*) measurement and potentiodynamic polarization test were carried out in SAR (open to air) at 25 ± 1 ^oC using a potentiostat (Princeton Applied Research, Versastat II) according to ASTM Standard G5-92 [46].

To simulate the acid rain, SAR was used for the corrosion test with compositions of SO_4^{2-} 15.2 mg/L, NO_3^- 11 mg/L, Cl^- 27.3 mg/L, Na^+ 27.3 mg/L, Ca^{2+} 5.5 mg/L, H^+ = 0.3 mg/L at pH 3.5 [47]. For all potential measurements, a saturated calomel electrode (SCE, +0.244V versus SHE at 25 ^oC) was used as the reference electrode. For measuring the current, 2 graphite rods were used as the counter electrodes. After the *OCP* measurement for 120 minutes, the potential was then increased from 0.2 V_{SCE} below the *OCP* at a rate of 0.0167 mV/min. The corrosion current density (I_{corr}) were extracted from the polarization curve by Tafel extrapolation using a commercial software (PowerCorr, V.2.42). Three replicate samples were used in running the polarization test for each kind of sample. After the polarization test, the corrosion morphologies of the samples were also investigated using SEM.

2.4 Electrical wear test

Electrical sliding wear tests for the laser-alloyed samples and cp Cu were performed using a pin-on-disc tribometer as shown in Fig. 2. The surface roughness

of the as-fabricated laser-alloyed samples was measured to be about 40 μm. In order to minimize the effect of the rough surface on the wear performance, the surfaces of the laser-alloyed samples and cp Cu were finally polished with the 1-μm diamond paste prior to the electrical wear test. A high-speed electrical motor was used to drive a large rotating disc with diameter of 420 mm for achieving a sliding speed of 60 km/h. The sample (the pin) was connected as the cathode and a electric current of 60 A was provided to it with a DC power supply. With a hydraulic press, a normal load of 50 N was exerted on the sample for keeping contact with the disc. The sample was forced to slide against a counterface tool steel rotating disc with hardness of 600 $HV_{0.2}$. In a third-rail system, Cu is often used as the current collector shoes and steel is used as the third rail for providing electricity. Also, the Fe-base contact strips (pantograph) are used in some catenary systems [48]. In the present study, tool steel was chosen as its hardness was comparable to that of the laser-alloyed samples. The total sliding distances for cp Cu and the laser-alloyed samples were 1 km and 20 km respectively.

In dry condition, the tests were conducted in air at ambient temperature of 25 ^{o}C and R.H. of 60%. In wet conditions, deionized water (DW) at pH 7 or SAR at pH 3.5 was added in drops near the contact surface at a rate of 0.5 mL/s. Owing to the existence of water and electric current, electric arc was produced resulting in arc erosion. The weight loss ΔW (in g) of the samples was intermittently recorded at a time interval of 1 minute using an electronic balance with an accuracy of $\pm$0.1 mg. All tests were repeated at least three times to ensure the repeatability of the experimental data under the same conditions. The experimental error of weight measurement was about 2.4%. The average wear loss (thickness loss) Δd was calculated by:

$$\Delta \text{d (mm)} = 10\frac{\Delta \text{W}}{\rho A} \qquad (4)$$

where ρ (g/cm^3) is the density and A (cm^2) is the exposed surface area of cp Cu or the laser-alloyed layers. The calculation of the densities of the laser-alloyed layers was based on the weight fractions of Cu, Ni, Ti and TiO_2 by the rule of mixture:

$$\frac{1}{\rho} = \frac{W_{Cu}}{\rho_{Cu}} + \frac{\text{W}_{\text{Ni}}}{\rho_{Ni}} + \frac{W_{Ti}}{\rho_{Ti}} + \frac{W_{TiO_2}}{\rho_{TiO_2}} \qquad (5)$$

where ρ_{Cu} = 8.94 g/cm^3 , ρ_{Ni} = 8.90 g/cm^3, ρ_{Ti} = 4.51 g/cm^3 and ρ_{TiO2} = 4.23 g/cm^3 are the theoretical densities of Cu, Ni, Ti and TiO_2 respectively, and the weight fractions of Cu, Ni and Ti in the laser-alloyed layer are W_{Cu}, W_{Ni}, W_{Ti} and W_{TiO2} respectively ($W_{Cu} + W_{Ni} + W_{Ti} + W_{TiO2} = 1$).

The wear rates of materials in dry condition (D), DW without electrochemical corrosion (E) and wear-corrosion rate in SAR (T) were calculated using:

$$\text{Wear rate (mm/h)} = \frac{\Delta d}{\Delta t} \qquad (6)$$

where Δt (in h) is the duration of the wear test.

Synergistic effect between electrical wear and corrosion of the laser-alloyed samples in SAR was analyzed. The wear-corrosion synergism S between electrical wear and corrosion was calculated using [49, 50]:

$$S = T - E - C \qquad (7)$$

where C is the corrosion rate of the samples in SAR calculated from I_{corr} according to ASTM Standard G102-89 [51]:

$$\text{C (mm yr}^{-1}) = K\left(\frac{I_{corr}}{\rho}\right)\text{EW} \qquad (8)$$

where K is a constant = 3.27 x 10^{-3} mm g μA^{-1} cm^{-1} yr^{-1}; I_{corr} is the corrosion current density in μA cm^{-2}; ρ is the density obtained from equation (5) in g cm^{-3} and EW is the equivalent weight, which is defined as follows:

$$EW = \left(\Sigma \frac{n_i W_i}{A_i} \right)^{-1} \quad (9)$$

where W_i is the weight fraction; n_i is the valence; and A_i is the atomic mass of the i^{th} element in the sample.

After the electrical sliding wear tests, the worn surface of the samples were analyzed using SEM and EDX, while the phase constitution was identified using XRD.

3. Results and discussion

3.1 Microstructure

The cross-sectional views and the compositional profiles along the depth of the laser-alloyed layers are shown in Fig. 3 and Fig. 4 respectively. The thickness of the layers was in the range of 0.53 to 0.85 mm (Table 1). The overall compositions of cp Cu, NiTi plate and the laser-alloyed samples are summarized in Table 2. For the double-layer samples fabricated at lower scanning speeds (i.e. LA-NiTi-Cu-25-25 and LA-NiTi-Cu-35-35), the thickness of the alloyed layers is larger and the Ni and Ti contents are lower. Among the double-layer samples, the thickness of LA-NiTi-Cu-35-45 is the smallest (Table 1) and dilution ratio is the lowest. To further reduce the dilution ratio and maintain high Ni and Ti contents, a third layer was fabricated on the surface of LA-NiTi-Cu-35-45 at 45 mm/s (the sample is designated as LA-NiTi-Cu-35-45-45). All alloyed layers were bonded metallurgically on the base metal without any porosity and crack.

From the XRD patterns (Fig. 5), the intermetallic phases (IMPs) of Ni-Ti and Cu-Ti, metallic phase [α-CuNiTi and NiTiCu (B19')] and metal oxides were detected in the alloyed layers (Table 2). For the double-layer sample fabricated at the lowest speed (i.e. LA-NiTi-Cu-25-25), α-CuNiTi is the major phase with martensitic NiTiCu

(B19'), $(NiCu)_3Ti$, CuTi, $TiO_2/NiTiO_3$ as the minor phases. During LSA, NiTi was so reactive that trace oxygen was picked up although the process was Argon-shielded. TiO_2 and $NiTiO_3$ were also detected as the minor phases. On the other hand, for the double-layer samples LA-NiTi-Cu-35-35 and LA-NiTi-Cu-35-45, their compositions and the phases present were found to be similar, both containing $(NiCu)_4Ti_3$ as the major phase with minor phases including martensitic NiTiCu (B19'), $(NiCu)_3Ti$, CuTi and $TiO_2/NiTiO_3$. $(NiCu)_4Ti_3$ is the intermediate/metastable phases formed before the formation of $(NiCu)_3Ti$ [52-54]:

$$L \rightarrow L + NiTiCu \rightarrow NiTiCu + (NiCu)_4Ti_3 \rightarrow NiTiCu + (NiCu)_3Ti$$

For the triple-layer sample LA-NiTi-Cu-35-45-45, the desirable martensitic NiTiCu (B19') appeared to be dominant with some minor phases of IMPs $(NiCu)_4Ti_3$, $(NiCu)_3Ti$, CuTi and $TiO_2/NiTiO_3$.

During irradiation of the samples by the HPDL, the preplaced NiTi powder absorbed the laser energy and melted instantaneously. Heat conduction and convection from the melted NiTi powder resulted in melting of the superficial cp Cu substrate. With the large temperature gradient (10^2 to 10^4 K/mm) between the center of the melt pool and the cooler solid-liquid interface [55, 56] and surface tension, Marangoni convective fluid flow led to mixing of the molten metals in the alloyed layer. From the BSE micrographs, three distinct phases with different contrasts (white, grey and black) are observed in the different alloyed layers (Fig. 6) and their compositions are shown in Table 3. Dendrites were finely dispersed in the layer and the microstructure was quite homogeneous in the alloyed layers. Similar microstructure was observed in the rapidly solidified $Ti_{49}Ni_{51-x}Cu_x$ (x = 5, 15, 25) at cooling rates of 10^2–10^3 K/s [28]. For the samples LA-NiTi-Cu-25-25, LA-NiTi-Cu-35-35 and LA-NiTi-Cu-35-45 in the present study, the white phases are

Cu-rich with lower Ni and Ti contents and low O content. On the other hand, the grey phases possess a lower Cu content but higher Ni and Ti contents as compared to the white phases. On the other hand the dark phases appear to be rich in Ti and O with smaller amount of Ni and Cu.

3.2 Hardness and elastic recovery ratio

Hardness profiles obtained along the cross-sections of the laser-alloyed samples are depicted in Fig. 7(a) and average hardness values (before wear test) are shown in Table 4. The hardness in the laser-alloyed layers is quite uniform and much higher than that of cp Cu (75±2 $HV_{0.2}$). Average hardness values of LA-NiTi-Cu-35-35 (455±17 $HV_{0.2}$) and LA-NiTi-Cu-35-45 are very close (465±22 $HV_{0.2}$) and higher than that of the laser-alloyed Cu with 60-wt% W (LA-W-Cu-p2, 150±26 $HV_{0.2}$) [39] but lower than of the laser-alloyed Cu with 70-wt% Ti (LA-Ti-Cu-20, 661±41 $HV_{0.2}$) [38] according to the previous studies of the present authors (Table 4). The enhanced hardness of LA-NiTi-Cu-35-35 and LA-NiTi-Cu-35-45 is due to the presence of hard IMP $(NiCu)_4Ti_3$ as the major phase in the laser-alloyed layers. Gao and Wang reported that the NiTi (B19') with $NiTi_2$ has higher hardness due to the presence of $NiTi_2$ [57-59]. On the other hand, it can be noticed that the triple-layer sample LA-NiTi-Cu-35-45-45 (435±43 $HV_{0.2}$) is not as hard as that of double-layer sample LA-NiTi-Cu-35-45 (465±22 $HV_{0.2}$) (Table 4) but harder than that of the NiTi plate (B2) (346±18 $HV_{0.2}$). It is attributed to existence of the softer major phase B19' in LA-NiTi-Cu-35-45-45. Among the laser-alloyed samples, the hardness of LA-NiTi-Cu-25-25 is the lowest (240±11 $HV_{0.2}$) due to the high dilution ratio and existence of the softer α-CuNiTi as the major phase.

Fig. 7(b) depicts the nanoindentation curves measured at the surface of various samples. All the laser-alloyed samples are more elastic than cp Cu, as indicated by the

larger elastic recovery ratios (Table 4). The elastic recovery ratios of the laser-alloyed samples were reduced by 30% to 55% as compared with the NiTi plate. For instance, the reduction of recovery ratio of LA-NiTi-Cu-25-25 is (42%-19%)/42% = 55%. The triple-layer sample LA-NiTi-Cu-35-45-45 possessed the highest elastic recovery ratio, indicating its shape memory effect has retained while the hardness is also enhanced. As α-CuNiTi is the major phase present in LA-NiTi-Cu-25-25, its shape memory property is the lowest among the laser-alloyed samples.

3.3 Electrochemical behavior

Fig. 8 shows the plots of *OCP* against time and potentiodynamic polarization curves of the various samples in SAR (open to air) at 25 ^{o}C. The *OCP* and I_{corr} are extracted and shown in Table 4. It can be observed that the *OCP* values of all laser-alloyed samples are nobler than those of cp Cu and the NiTi plate while the I_{corr} values of the former group are in between the latter group.

In SAR (pH 3.5), cp Cu is nobler while the NiTi plate is more active but self-passivating as shown in Fig. 8. It could be seen that the NiTi plate showed passivation (Fig. 8b). Its anodic current density remained constant as it was polarized to a nobler potential. Passivation of the NiTi plate in an acidic media was attributed to the existence of the uniform oxide layer. Figueira and his co-workers demonstrated that the passive behavior for NiTi has no significant differences at pH values of 3, 5.7, 7.4 and 10 [60]. In the present study, the protective oxide film of the laser-alloyed samples increased the corrosion rates or I_{corr}.

It is interesting that the *OCP* of all laser-alloyed samples in SAR are slightly higher than that of cp Cu and NiTi alloy. The noble shift in the *OCP* for all laser-alloyed samples shows their thermodynamic stability in SAR. This finding is consistent with that obtained from Chang and Chui [61] and Wen and his co-workers

[62] who reported that the presence of Cu in the Ti-Ni-Cu alloys could shift their corrosion potentials ~~to~~ in the noble direction but more Ni and Cu ions were selectively leached. Among the laser-alloyed samples, the *OCP* of LA-NiTi-Cu-25-25 which consists of α-CuNiTi (with the highest Cu content) is noblest, followed by the *OCP* of LA-NiTi-Cu-35-35 and LA-NiTi-Cu-35-45 which contain $(NiCu)_4Ti_3$ (with lower Cu content). While the *OCP* of LA-NiTi-Cu-35-45-45 is the most active among the laser-alloyed samples but still higher than those of the NiTi plate and cp Cu. In addition, the corrosion rates of Cu-Ni alloys decreased with the increase in Ni content up to 30 wt.% in the acidic chloride solution [63]. The noble shift in their corrosion potentials was due to the incorporation of Ni ions into the Cu_2O film. It was more corrosion resistant than the undoped Cu_2O film.

The I_{corr} values of all laser-alloyed samples are larger than that of NiTi plate but smaller than that of cp Cu. Selective leaching rates of Ni and Cu ions in NiTiCu was higher than that of the NiTi alloy due to the formation of NiO and Cu_2O, thus decreasing the uniformity of the TiO_2 passive layer [61].

The presence of the IMPs/oxides leading to a non-uniform passive oxide layer in the laser-alloyed samples is the major cause of higher I_{corr} as compared with the NiTi plate. The corrosion rates of the laser-alloyed layers increase with the increase in Cu content, as evidenced by a higher corrosion rate for LA-NiTi-Cu-25-25 with the highest *DR* (i.e. the highest Cu content) (Fig. 9a). The laser-alloyed samples are not as corrosion resistant as NiTi plate, but more corrosion resistant (i.e. lower I_{corr}) than that of cp Cu. According to the values of I_{corr} in Table 4, the corrosion resistance ranking in SAR is:

NiTi plate > LA-NiTi-Cu-35-45-45 > LA-NiTi-Cu-35-45 > LA-NiTi-Cu-35-35 > LA-NiTi-Cu-25-25 > cp Cu

Among all laser-alloyed samples, LA-NiTi-Cu-35-45-45 was the most corrosion

resistant because of the highest Ni and Ti contents and formation of uniform passive oxide film. In short, increase in Ni and Ti contents in the alloyed layers leads to decrease in I_{corr}. The corroded morphology of LA-NiTi-Cu-35-45-45 with the highest Ti and Ni contents after polarization tests in SAR revealed that only mild corrosion is observed (Fig. 9b). According to the Pourbaix diagram of copper-water system [64], cp Cu is active in acidic media, thus, having the highest corrosion tendency among all the samples. Compared with the laser-alloyed Cu with W [40] and the laser-alloyed Cu with Ti [38], LA-NiTi-Cu-35-45-45 is the noblest and its I_{corr} is the lowest in SAR as shown in Table 4. According to the values of I_{corr}, the ranking of corrosion resistance of the laser-alloyed Cu with NiTi, Ti and W in SAR is:

NiTi plate > LA-NiTi-Cu-35-45-45 > LA-W-Cu-p2 > LA-Ti-Cu-20 > cp Cu

However, LA-NiTi-Cu-35-45-45 does not show considerable passivity (Fig. 8b). Compared with the NiTi plate, the oxide layers of the laser-alloyed samples were not uniform and stable enough against corrosion attack. Moreover, the presence of the IMPs/oxides may act as initiation sites for corrosion attack. It is reported that rapid solidification of the melt pool during LSA of NiTi powder and laser cladding of NiTi strip on 316L substrate leading to the inhomogeneous alloyed layers [27]. The inhomogeneity could lead to an imperfect passive film and acts as initiation sites for pitting corrosion [61]. A local breakdown of the oxide layer of the laser-alloyed samples initiated corrosion attack due to preferable adsorption of the chloride ions on their surface and consequently hindered repassivation of the oxide at localized regions.

3.4 Electrical sliding wear behavior

The plots of cumulative thickness (wear) loss against sliding distance for various samples under different environmental conditions are shown in Fig. 10. The average

wear rates in air (*D*), in DW (*E*) and in SAR (*T*), wear-corrosion synergism (*S*) and corrosion rate in SAR (*C*) are depicted in Fig. 11 and Table 5. Compared to cp Cu, the laser-alloyed samples show significant drop in the wear rates (*D*, *E* and *T*). During electrical wear, the surface oxide formed on the samples could effectively reduce the wear loss due to abrasive and adhesive wear [57]. The ranking of electrical wear resistance of various samples is:

LA-NiTi-Cu-35-45-45 > LA-NiTi-Cu-45-45 > LA-NiTi-Cu-35-35 >

LA-NiTi-Cu-25-25 >> cp Cu

Moreover, the ranking of wear rates in different conditions, synergism and corrosion contribution in SAR are:

$$D > T > E > S >> C$$

For the laser-alloyed samples, *S* shows a small contribution to *T* whereas *C* is negligible as compared with *D, T* and *E* as shown in Table 6.

Among the laser-alloyed samples, LA-NiTi-Cu-35-45-45 shows the lowest cumulative thickness loss. On the contrary, the cumulative thickness loss of LA-NiTi-Cu-25-25 is the highest due to the presence of the major phase α-CuNiTi with lower hardness (Fig. 10). In the previous studies of Kwok's group, the electrical sliding wear behavior of the laser-alloyed Cu with W (60 wt%, designated as LA-W-Cu-p2) [39] and the laser-alloyed Cu with Ti (70 wt%, designated as LA-Ti-Cu-30) [39] in dry and wet conditions was reported. The ranking of electrical wear resistance of laser-alloyed Cu with different alloying elements in dry and wet conditions is:

LA-NiTi-Cu-35-45-45 > LA-W-Cu-p2 > LA-Ti-Cu-30 > > cp Cu

In the dry condition, the electrical wear resistance of Cu laser-alloyed with NiTi is superior to those of Cu laser-alloyed with W / Ti by 14.5 / 19.5 times and higher than that of cp Cu by three orders of magnitude. In particular, the wear resistance of

LA-NiTi-Cu-35-45-45 has improved by 3663 times when compared to cp Cu, which was severely damaged after sliding for 1 km in air.

From Fig. 11, although LA-NiTi-Cu-35-45-45 is not the hardest, it is the most wear resistant among the laser-alloyed Cu with NiTi. For the laser-alloyed Cu with W reported by Kwok's group, the immiscible micro-sized W particles are uniformly distributed in the Cu matrix [39]. The hard W phase could withstand the load and wear loss was reduced. In addition to the increase in hardness, the high softening temperature of W can also help to resist in material loss during electrical sliding wear. The presence of tungsten oxide film could also reduce abrasive and adhesive wear loss. The improved electrical wear resistance of the laser-alloyed Cu with Ti with dendritic structure is attributed to the combined effect of the hard Cu-Ti IMPs and solid solution strengthening [38]. For the conventional tribo-materials, hardness is a major factor that affects the electrical wear resistance. The hard IMPs in the laser-alloyed layers could decrease the load transferring to the Cu binder, and the laser-alloyed layers mainly withstood the applied load [65]. Apart from the hard IMPs, the surface oxide could act as lubricant and effectively reduce the wear. In addition, particle strengthening (oxide particles) and composite strengthening (pick up of counter material or wear particles) during electrical wear could help to strengthen the laser-alloyed coatings [66, 67]. In the present study, the superior electrical wear resistance of LA-NiTi-Cu-35-45-45 is mainly attributed to pseudo-elasticity. Yan reported that the high wear resistance of NiTi (B19') was due to the low Young's modulus [68]. It allowed B19' to have a rubber-like behavior, low transformation stress, high recoverable transformation strain and high yield strength which were important in hindering plastic deformation. In addition to the pseudo-elastic effect for accommodating deformation, the hard IMPs also assisted in withstanding external load, the work hardening effect and formation of oxides may also help in enhancing

the electrical wear resistance.

In general, all laser-alloyed samples have higher wear loss in dry condition than in wet condition. In dry condition, frictional heat generated between the samples and the counterface disc led to softening of the samples and hence greater wear loss. On the contrary, with the aid of the lubrication and cooling effects of DW and SAR, frictional heat generated was greatly reduced. From Fig. 11, the wear rate of the samples in dry condition is the highest, followed by SAR and then DW. In wet condition, water will facilitate the formation of cuprous oxide which may act as a lubricating protective layer in between the sliding couple. It can be perceived that the corrosive effect of SAR has only a minor contribution to the wear process.

The wear loss of the laser-alloyed Cu with NiTi is much smaller than that of cp Cu as revealed by the cross-sectional view of the worn samples after sliding in dry and SAR conditions (Fig. 12 and Fig. 13) and very few worn debris has been collected. There is only a small reduction in thickness of the alloyed layer after electrical sliding wear.

Compared with the conventional tribo-materials, NiTi alloys have been reported to exhibit very high wear resistance due to their good combination of pseudo-elasticity, ductility and toughness [9-14]. Their superior wear resistance can be attributed to three main factors, namely pseudo-elasticity of NiTi, hard phases/NiTi matrix hardening effect and work hardening effect. Such effects on the electrical wear behavior of the laser-alloyed samples are discussed as follows.

3.4.1 Pseudo-elasticity and Pseudo-plasticity

According to the literature, the high wear resistance of the ternary NiTiCu alloy could be attributed to the pseudo-elasticity of B2 and the pseudo-plasticity of B19’ [28-31, 68-69]. In the present study, only B19’ was found in the laser-alloyed Cu with

NiTi, thus the wear mechanism of B19’ will be discussed. Deformation of twinned B19’ can be summarized to four stages [69-71] including (i) elastic deformation of twinned martensite; (ii) martensite detwinning; (iii) elastic deformation of detwinned martensite; (iv) plastic deformation of detwinned martensite. The self-accommodating martensite reoriented along the stress direction during loading a NiTiCu alloy in pseudo-plastic state [71-73]. The alloy was pseudo-plastically deformed when most or all the martensites were arranged in one orientation.

3.4.2 Hard intermetallic phases / NiTiCu matrix hardening effect

In addition to B19’, the IMPs present in the laser-alloyed layer forming a composite layer could resist wear. The hard IMPs can withstand external load whereas the ductile B19’ phase could accommodate deformation and bind the IMPs for resisting cracking. Existence of the IMP Ni_4Ti_3 in the NiTi alloy could significantly improve the hardness, yield strength and fatigue resistance [74-79]. On the other hand, other researchers [23, 57-59] reported that the IMPs $NiTi_2$ and Ni_3Ti could impede the shear plastic deformation. However, these hard but brittle IMPs initiated the cracks. When the hard IMPs are present in the NiTiCu matrix, initiated cracks are prohibited due to the excellent ductility of NiTiCu. Li reported that sintered TiC-NiTi samples contained porosities, but their wear resistance was comparable to that of the WC-NiCrBSi [78]. So the wear resistance of ductile NiTiCu incorporated with the hard IMPs could be highly improved.

3.4.3 Work hardening effect

The hardness of the worn surface of the laser-alloyed samples after the electrical sliding wear test in dry condition is noticeably harder than that before the wear test as shown in Table 4. The harder worn surface is due to the plastic deformation and

strong work hardening of the surface during the electrical sliding wear test. Similar result was obtained by Gao and his co-workers who reported hardening of the surface of the laser melting/deposited Ti_2Ni/TiNi intermetallic alloy after dry sliding wear [57-59]. The surface hardness of such alloy was found to be increased from 310 to 420 $HV_{0.2}$ reflecting the strong work hardening effect after dry wear.

Compared with cp Cu, the wear rates of the laser-alloyed Cu with NiTi are dramatically reduced by 3 orders of magnitude in all conditions (Fig. 11). The laser-alloyed sample (LA-NiTi-Cu-35-45-45) with B19' as the major phase possessed the highest electrical wear resistance, whereas the resistance of LA-NiTi-25-25 with the high Cu content was the lowest. It is noticeable that both LA-NiTi-Cu-35-35 (455±17 $HV_{0.2}$) and LA-NiTi-Cu-35-45 (465±22 $HV_{0.2}$) are harder than LA-NiTi-Cu-35-45-45 (435±43 $HV_{0.2}$) but the electrical wear resistance of the former is relative low. It was reported that hardness was not the only factor responsible for the high wear resistance of the NiTi alloy [13]. The wear resistances of the laser-alloyed samples are dominated by the pseudo-plasticity rather than the hardness of the IMPs.

3.4.4 Electrical wear in dry condition

From the plots of cumulative wear loss vs time (Fig. 10) and wear rates of various samples under different conditions (Fig. 11), the wear loss of all samples in dry condition is more than that in wet conditions. For dry wear, the frictional heat generated between the samples and the counterface steel disc can only be dissipated in the surrounding environment. From the Archard's equation, electric current would cause Joule heating which further softened the samples leading to greater wear loss [79]. When sliding with electric current, both frictional heating and Joule heating exist and the total power of heating is the sum of both origins:

$$P = I^2R_c + \mu vF \qquad (10)$$

where I is the electric current, R_c is the contact resistance, μ is the friction coefficient, v is the sliding speed and F is the normal load applied to the samples. Electrical wear behavior of cp Cu in dry and wet conditions has been reported elsewhere [38, 70]. cp Cu was softened and massive amount of material transfer and oxidation occurred as evidenced by adhesive Cu patches attached on the steel counterface.

In the present study, less severe worn morphology was observed from the worn surfaces of the laser-alloyed samples as shown in Fig. 12 but surface cracks are observed in some laser-alloyed samples after the wear test. During electrical sliding wear, hard and brittle oxides were formed and served as lubricant at the early stage. However, as the temperature increases, the strength of the oxide layer decreases leading to fracture and detachment [80]. The detached oxides acted as hard abrasive and consequently abrasive wear occurred. The surface cracks show that oxidation occurred in between the sliding surfaces. However, no internal crack was observed along the cross-section of the laser-alloyed samples after the wear test. This could be attributed to the excellent ductility and toughness of the alloyed layer (NiTiCu) which prevented the hard and brittle IMPs from fracture. The present finding is consistent with that observed by Gao and his co-workers [57-59, 75], who reported the propagation of cracks from IMP $NiTi_2$ were prevented in the NiTi phase. From the worn surface of the laser-alloyed samples after electrical wear in dry condition, the degree of wear damage and susceptibility to surface cracking of triple-layer sample (LA-NiTi-Cu-35-45-45) were less severe than those of the double-layered samples (LA-NiTi-Cu-25-25, LA-NiTi-Cu-35-35 and LA-NiTi-Cu-35-45).

Another evidence for the high wear resistance of the laser-alloyed samples is that only a small amount of Fe was detected on the worn surface from the counterface steel disc (Fig. 12). From the XRD results of the worn surface [Fig. 14(a)(i) & (b)(i)],

Fe_2O_3 was detected confirming adhesive wear of the steel disc occurred. Moreover, other oxide peaks were detected. It was reported that surface oxides could act as solid lubricant between the sliding surfaces and could reduce wear to some degree [57-59]. Bateni and his co-workers reported that TiO_2 on the surface of Ti-Cu coatings on cp Cu formed by pack cementation could reduce the wear loss effectively in dry condition because it acted as a solid lubricant in between the sliding surfaces [65].

By using thermography, the maximum temperature of LA-NiTi-Cu-35-45-45 worn in dry condition is approximately 97 ^{o}C. However, it is expected that the temperature caused by frictional heat and Joule heating may even be higher at the real contact between the samples and the counterface steel disc. On the other hand, when the applied load exceeded the yield strength of the detwinned martensite, dislocations were accumulated and plastic deformation then occurred [79]. From the TEM micrographs of the LA-NiTi-Cu-35-45-45 before and after electrical wear test in dry condition (Fig. 15), the dislocation densities were greatly increased after the test. This showed that the applied stress could reach the yield strength of the detwinned martensite resulting in material loss.

3.5.5 Electrical wear in wet condition

With the effects of cooling and lubricating of DW and SAR, the frictional heat generated was greatly reduced during electrical wear. From Fig. 11, the wear rates of the samples are the lowest in DW, followed by SAR and the highest in dry wear. The worn surfaces of the laser-alloyed samples after sliding in SAR are shown in Fig. 13. This shows that the reduction in temperature and frictional heat can greatly reduce the wear loss. Shangguan and his co-workers [820] reported that there was a greater amount of oxygen detected on the surface under wet conditions than that in dry condition when sliding copper against a copper-alloy counterpart under a current of

100 A.

In the wet conditions, water facilitated the formation of cuprous oxide which may act as a lubricating protective layer in between the sliding couple. The present finding is consistent with that of Shangguan et al [82]. Cuprous oxide would be formed on the surface of the laser-alloyed copper with NiTi with the water and acted as a lubricating protective layer against electrical wear. Besides, it could be noticed that the number of cracks on the surface of the laser-alloyed samples after the test was greatly reduced in wet conditions.

It could be perceived that the effect of corrosion on electrical wear of the laser-alloyed Cu with NiTi in SAR was minor. The present finding was different from those obtained by Li [78] who performed sliding wear tests for TiC-NiTi, NiTi and WC-NiCrBSi samples in air, 2% H_2SO_4 solution, tap water and 2% NaCl solution with applied load up to 200 N and sliding speed of 3.6 km/h. Li claimed that the volume losses in dry wear, tap water and 2% NaCl solution were very similar. While the volume loss in 2% H_2SO_4 and was almost 2 times higher as compared to the loss in other media. It is because the SAR (pH = 3.5) used in the present study was less corrosive than the 2% H_2SO_4 (pH = 0.57). The corrosion effect of the SAR was not obvious despite the existence the IMPs and oxides. However, Li reported that the volume loss in dry sliding is similar to those in tap water [79], such inconsistency with the present finding may be attributed to lower sliding speed used in the wear test done by Li. Even though the reinforcing particles caused microstructural inhomogeneity, the TiC-NiTi composite was more wear resistant than the NiTi alloy in corrosive medium. Actually, the reinforcing particles did not significantly affect the corrosion resistance of the NiTi alloy [79].

The contributions of *E* (in DW), *C* and *S* to total wear rate *T* (in SAR) of the samples are shown in Table 5. The high percentages of *E/T* for all samples indicate

that the wear loss is mainly caused by mechanical and arcing effects. The corrosivity of the SAR could increase wear loss by wear-corrosion synergism (*S*) as reflected by the higher wear rate (*T* > *E*). The synergism effect can reach up to 36.1% for the laser-alloyed Cu with NiTi. The wear loss in SAR consisted of detachment of fine wear debris and corrosion products. When the corrosion products were removed, a fresh surface would be exposed to the SAR for further attack. This cycle would repeat throughout the test. In short, the higher wear rate of the laser-alloyed samples SAR was attributed to the synergistic effect of mechanical wear, arc erosion, and wear-corrosion synergism caused by SAR, whereas effect of corrosion (*C*) is insignificant.

3.5 Interfacial contact resistance

Fig. 16 depicts the plot of *ICR* of cp Cu and the laser-alloyed Cu with NiTi, Ti and W vs applied compressive force per unit area. Table 4 shows the steady values of *ICR* at 50 N/cm^2 and the *ICR* ranking is:

LA-W-Cu-p2 > LA-NiTi-Cu-35-45-45 ~ LA-Ti-Cu-30 > LA-NiTi-Cu-35-45 ~ LA-NiTi-Cu-35-35 > LA-NiTi-Cu-25-25 > cp Cu

Among all laser-alloyed samples, the *ICR* of LA-NiTi-Cu-25-25 is the lowest due to the highest Cu content in the laser-alloyed layer. In contrast, the *ICR* of LA-W-Cu-p2 is the highest due to the high electrical resistance of W [40]. Compared with cp Cu, the *ICR* of the laser-alloyed Cu with NiTi has increased by 3.5-7.2 times at 50 N/cm^2. With the decrease in *DR*, the electrical sliding wear and corrosion resistances increase, on the contrary, the electrical conductivity will be lower. Although the *ICR* of LA-NiTi-35-45-45 is the highest among the laser-alloyed samples, it possesses the highest electrical wear and corrosion resistances. The resistivities of Ni (70 nΩ • m) and Ti (420 nΩ • m) are higher than that of Cu (17 nΩ • m). As the Ni and Ti contents

increases from 25 to 85 wt%, the *ICR* of the laser-alloyed samples increase to 0.109 – 0.223 $m\Omega \cdot cm^2$ (about 3.5 – 7.2 times that of cp Cu). It was reported that a 80-μm sandwich layer of Mo–Ni-Cu on Cu formed by laser cladding possessed a specific contact resistance of about 0.0563 $m\Omega \cdot cm^2$ (the resistivity of Mo is 53 $n\Omega \cdot m$) [83]. Compared with the laser-cladded Cu with Mo-Ni, the higher *ICR* of the laser-alloyed Cu with Ti is attributed to the higher resistivity of Ti and the much thicker alloyed Cu-Ti layers (350 – 800 μm). To enhance wear resistance, 2.5 wt.% TiB_2 was added to Cu and the electrical resistivity was increased by a factor of 8 [84]. The ceramic phase TiB_2 in Cu-TiB_2 composites and similarly the intermetallic phases in the laser-alloyed Cu-Ti acted as scattering centers and the electricity resistivity increased with the concentration of Ti or TiB_2 in the alloys or composites [83, 84]. In the present study, besides the alloying elements (Ni and Ti), the existence of some TiO_2 with high resistivity (10^{12} Ω.cm) in the laser-alloyed samples would increase the *ICR*.

A radar diagram (Fig. 17) is used to compare the various samples including cp Cu, LA-NiTi-Cu-35-45-45, LA-Ti-Cu-30 [39] and LA-W-Cu-p2 [40] with respect to their electrical conductivity, electrical sliding wear and corrosion resistances, hardness and cheapness. Among the various samples, the *ICR* of cp Cu has the lowest, thus it is graded as the highest ranking. Whereas *ICR* of LA-W-Cu-p2 is the highest and its ranking is the lowest. As low cost is also an important factor that may affect the decision of material selection, the coating materials with the lowest price will be preferable. Aside from the price, LA-W-Cu-p2 and LA-Ti-Cu-20 have almost all properties inferior to that of LA-NiTi-Cu-35-45-45. Thus, it can be concluded that LA-NiTi-Cu-35-45-45 can be a good candidate as an electric contact material.

4 Conclusions

- The laser-alloyed Cu with NiTi mainly consist of NiTiCu (B19'), $(NiCu)_4Ti_3$,

$(NiCu)_3Ti$ and CuTi), oxide (TiO_2) and metallic phase α-CuNiTi. α-CuNiTi is only detected in the double-layer sample fabricated at the lowest scanning speed. Moreover, the sample with triple-layers (LA-NiTi-Cu-35-45-45) has the lowest dilution ratio and contains B19' as the major phase.

- All laser-alloyed Cu with NiTi possess higher surface hardness (240±11 to 465±22 $HV_{0.2}$) than that of cp Cu (75±2 $HV_{0.2}$). In particular, the hardness of LA-NiTi-Cu-35-45 is the highest owing to the presence of hard IMPs $(NiCu)_4Ti_3$, $(NiCu)_3Ti$ and CuTi.
- The corrosion resistance of the laser-alloyed samples is higher than that of cp Cu in SAR. According to I_{corr}, the ranking of corrosion resistance is: LA-NiTi-Cu-35-45-45 > LA-NiTi-Cu-35-45 > LA-NiTi-Cu-35-35 > LA-NiTi-Cu-25-25 > cp Cu
- The cumulative wear loss of the laser-alloyed samples is much lower than that of cp Cu in dry and wet conditions. Their improved wear resistance is due to the presence of pseudo-plasticity of B19' and hard IMPs, and work hardening effect during electrical wear.
- The electrical wear resistance of the laser-alloyed samples is higher in wet conditions than in dry condition owing to lubrication effect and reduction in frictional heat. Moreover, the number of surface cracks is reduced when sliding in wet conditions.
- The wear rates of the samples in different conditions are as follows:

$$D > T > E > S >> C$$

- The main contribution of electrical wear in SAR is mechanical wear (*E*), with contribution of wear-corrosion synergism (*S*) up to 36.1%, while corrosion (*C*) alone is negligible.
- The *ICR* of the laser-alloyed samples at 50 N/cm^2 has increased from 3.5 -

7.2 times as compared with cp Cu.

- Among the laser-alloyed Cu with W, Ti and NiTi, the one alloyed with NiTi possesses the highest electrical wear and corrosion resistances, making it a good candidate for electric contact applications in acid rain.

Acknowledgments

This work was supported by the Multi-Year Research Grant (MYRG) of University of Macau [Grant number MYRG2018-00217-FST].

References

[1] ASM Handbook (Vol. 2): Properties and selection: nonferrous alloys and special-purpose materials, ASM International, Materials Park, OH, 1990, 219, 529, 592.

[2] C.R.F. Azevedo, A. Sinatora, Failure analysis of a railway copper contact strip, Eng. Fail. Anal. 11 (2004) 829–841.

[3] Y. Oura, Y. Mochinaga, H. Nagasawam, Railway Electric Power Feeding Systems, Japan Railway & Transport Review 16 (1998) 48–58.

[4] A. Senouci, H. Zaidi, J. Frene, A. Bouchoucha, D. Paulmier, Damage of Surfaces in Sliding Electrical Contact Copper/Steel Appl. Surf. Sci. 144–145 (1999) 287–291.

[5] S.G. Jia, P. Liu, F.Z. Ren, B.H. Tian, M.S. Zheng, G.S. Zhou, Sliding wear behavior of copper alloy contact wire against copper-based strip for high-speed electrified railways, Wear, 262 (2007) 772–777.

[6] S. Kubo, K. Kato, Effect of arc discharge on wear rate of Cu-impregnated carbon strip in unlubricated sliding against Cu trolley under electric current, Wear, 216

(1998), 172–178.

[7] Guiming Mei Wenming Fu, Guangxiong Chen, Weihua Zhang, Effect of high-density current on the wear of carbon sliders against Cu-Ag wires, Wear, 452–453 (2020) 203275.

[8] J.P. Tu, W.X. Qi, Y.Z. Yang, F. Liu, J.T. Zhang, G.Y. Gan, N.Y. Wang, X.B. Zhang, M.S. Liu, Effect of aging treatment on the electrical sliding wear behavior of Cu-Cr-Zr alloy, Wear 249 (2002) 1021–1027.

[9] G. Rondelli, Corrosion resistance tests on NiTi shape memory alloy, Biomaterials (1996) 2003–2008.

[10] D.Y. Li, R. Liu, The mechanism responsible for high wear resistance of Psuedo-elastic TiNi alloy – a novel tribo-material, Wear 225-229 (1999) 777–783.

[11] P. Clayton, Tribological behavior of a titanium-nickel alloy, Wear 162-164 (1993) 202–210.

[12] Y.N. Liang, S.Z. Li, Y.B. Jin, W. Jin, S. Li, Wear behavior of a TiNi alloy, Wear 198 (1996) 236–241.

[13] D.Y. Li, A new type of wear-resistant material: pseudo-elastic TiNi alloy, Wear 221 (1998) 116–123.

[14] F.T. Cheng, K.H. Lo, H.C. Man, NiTi cladding on stainless steel by TIG surfacing process Part I. Cavitation erosion behavior, Surface and Coatings Technology 172 (2003) 308–315.

[15] N. Levintant-Zayonts, F. Starzynski, M. Kopec, S. Kucharski, Characterization of NiTi SMA in its unusual behavior in wear tests, Tribology International 137, (2019), 313–323.

[16] A. Ziolkowski, B. Raniecki, S. Miyazaki, Stress induced martensitic transformation kinetics of polycrystalline NiTi shape memory alloy, Mater. Sci.

Eng. A, 378 (2004) 86–91.

[17] J. Mohd Jani, M. Leary, A. Subic, M.A. Gibson, A review of shape memory alloy research, applications and opportunities, Mater Des, 56 (2014), 1078–1113

[18] M. Bendahan, P. Canet, J.L. Seguin, H. Carchano, control composition study of sputtered Ni-Ti shape-memory alloy film, Materials Science and Engineering B 34 (1995) 112–115.

[19] A.P. Jardine, Vacuum conditions for sputtering thin-film TiNi, Journal of Vacuum Science and Technology A13 (1995) 1058–1062.

[20] K.S. Zhou, D.Z. Wang, M. Liu, A study of the cavitation-erosion behavior of a Ti-Ni alloy coating, Surface and Coatings Technology 34 (1988) 79–87.

[21] J.L. He, K.W. Won, J.L. Chang, TiNi thin films prepared by cathodic arc plasma ion plating, Thin Solid Films 359 (2000) 46–54.

[22] R. H. Richman, A.S. Rao, D. Kung, Cavitation-erosion of NiTi explosively welded to steel, Wear 181-183 (1995) 80–85.

[23] H. Hiraga, T. Inoue, S. Kamado, Y. Kojima, A. Matsunawa, H. Shimura, Fabrication of NiTi intermetallic compound coating made by laser plasma hybrid spraying of mechanically alloyed powders, Surface and Coatings Technology 139 (2001) 93–100.

[24] K.Y. Chiu, F.T. Cheng, H.C. Man, Cavitation erosion resistance of AISI 316L stainless steel laser surface-modified with NiTi, Materials Science and Engineering A 392 (2005) 348–358.

[25] K.Y. Chiu, F.T. Cheng, H.C. Man, Laser cladding of austenitic stainless steel using NiTi strips for resisting cavitation erosion, Materials Science and Engineering A 402 (2005) 126–134.

[26] F.T. Cheng, K.H. Lo, H.C. Man, NiTi cladding on stainless steel by TIG surfacing process Part II. Corrosion behavior, Surface and Coatings Technology

172 (2003) 316–321.

[27] K.Y. Chiu, F.T. Cheng, H.C. Man, Corrosion behavior of AISI 316L stainless steel surface-modified with NiTi, Surface and Coatings Technology 200 (2006) 6054–6061.

[28] G. Pan, C. Balagna, L. Martino, J. Pan, S. Spriano, Microstructure and transformation temperatures in rapid solidified Ni-Ti alloys. Part II: The effect of copper addition, Journal of Alloys and Compounds 589 (2014) 633-642.

[29] O. Mercier, K.N. Melton, Substitution of Cu for Ni in NiTi shape memory alloys, Metallurgical Transactions A 10 (1979) 387-389.

[30] K. Chastaing, P. Vermaut, P. Ochin, C. Segui, J. Y. Laval, R. Portier, Effect of Cu and Hf additions on NiTi martensitic transformation, Materials Science and Engineering A 438-440 (2006) 661-665.

[31] W.J. Moberly, K.N. Melton, Ni-Ti-Cu Shape Memory Alloys, Engineering Aspects in Shape Memory Alloys (1990) 46-57.

[32] M. Callisti, F. D. Tichelaar, B.G. Mellor, T. Polcar, Effects of Cu on the microstructural and mechanical properties of supper deposited Ni-Ti thin films, Surface and Coatings Technology 237 (2013) 261-268.

[33] C. Tatar, R. Acar, I.N. Qader, Investigation of thermodynamic and microstructural characteristics of NiTiCu shape memory alloys produced by arc-melting method, Eur. Phys. J. Plus 135 (2020) 311.

[34] A. Hirose, K.F. Kobayashi, Surface alloying of copper with chromium by CO_2 laser, Materials Science and Engineering A 174 (1994) 199-206.

[35] J. Dutta Majumdar, I. Manna, Laser surface alloying of copper with chromium I. Microstructural evolution, Materials Science and Engineering A 268 (1999) 216–226.

[36] J. Dutta Majumdar, I. Manna, Laser surface alloying of copper with chromium II.

Improvement in mechanical properties, Materials Science and Engineering A 268 (1999) 227–235.

[37] P.K. Wong, C.T. Kwok, H.C. Man, F.T. Cheng, Corrosion behavior of laser-alloyed copper with titanium fabricated by high power diode laser, Corrosion Science 57 (2012) 228-240.

[38] C.T. Kwok, P.K. Wong, H.C. Man, Laser surface alloying of copper with titanium: Part I. Electrical wear resistance in dry condition, and Laser surface alloying of copper with titanium: Part II. Electrical wear resistance in wet and corrosive condition, Surface and Coatings Technology, Vol. 297, pp. 66-73 (2016).

[39] P.K. Wong, C.T. Kwok, H.C. Man, D. Guo, Laser fabrication of W-reinforced Cu layers: I. Corrosion behavior in 3.5% NaCl solution and synthetic acid rain, Materials Chemistry and Physics, 181, pp. 397-408 (2016).

[40] P.K. Wong, C.T. Kwok, H.C. Man, D. Guo, Laser fabrication of W-reinforced Cu layers: II. Electrical wear behavior in air and synthetic acid rain, Materials Chemistry and Physics, Vol. 177, pp. 118-130 (2016).

[41] G. Dehm, B. Medres, L. Shepeleva, C. Scheu, M. Bamberger, B.L. Mordike, S. Mordike, G. Ryk, G. Halperin, I. Etsion, Microstructure and tribological properties of Ni-based claddings on Cu substrate, Wear, 225-229 (1999) 18-26.

[42] J.M. Pelletier, A. Issa, P. Sallamand, Laser surface alloying on copper base alloys, Lasers in Engineering 2 (1993) 81-92.

[43] R. Jendrzejewski, G. Sliwinski, Investigation of temperature and stress fields in laser cladded coating, Applied Surface Science, 254 (2007) 921-925.

[44] J.M. Pelaprat, M. Finuf, R. Fritz, M. Zediker, Laser Focus World, Novel Lasers: Blue direct-diode lasers extend industrial laser capability, 2018. https://www.laserfocusworld.com/lasers-sources/article/16555269/novel-lasers-b

lue-directdiode-lasers-extend-industrial-laser-capability

[45] H.L. Wang, M.A. Sweikart, J.A. Turner, Stainless Steel as Bipolar Plate Material for Polymer Electrolyte Membrane Fuel Cells, Journal of Power Sources 115 (2003) 243-251.

[46] ASTM Standard G5-92: "Standard Reference Test Method for Making Potentiodynamic Anodic Polarization Measurement, ASTM Standards, Philadelphia, 1994.

[47] http://www.smg.gov.mo/www/ccaa/report/pdf/IQA_Y/IQA_2012.pdf

[48] H. Nagasawa, K. Kato, Wear mechanism of copper alloy wire sliding against iron-base strip under electric current, Wear 216 (1998), 179-183.

[49] Standard Guide for Determining Synergism Between Wear and Corrosion, G119-04, Annual Book of ASTM Standards, vol. 03.02, ASTM, Philadelphia, 2004.

[50] C.T. Kwok, F.T. Cheng, H.C. Man, Laser-fabricated Fe-Ni-Co-Cr-B austenitic alloy on steels. Part II. Corrosion behaviour and corrosion-erosion synergism, Surface and Coatings Technology 145 (2001) 206-214.

[51] Standard Practice for Calculation of Corrosion rates and Related Information from Electrochemical Measurement, G102-89, Annual Book of ASTM Standards, Vol. 03.02, ASTM, Philadelphia, 1995.

[52] K. Khanlari, M. Ramezani, P. Kelly, P. Cao, T. Neitzert, Synthesis of As-sintered 60NiTi Parts with a High Open Porosity Level, Materials Research, 2018, 21(5)

[53] B. Chad Hornbuckle, Xiao X. Yu, Ronald D. Noebe, Richard Martens, Mark L. Weaver, Gregory B. Thompson, Hardening behavior and phase decomposition in very Ni-rich Nitinol alloys, Materials Science and Engineering A 639, (2015), 336-344.

[54] B. Bertheville, M. Neudenberger, J.E. Bidaux, Powder sintering and

shape-memory behavior of NiTi compacts synthesized from Ni and TiH_2, Materials Science and Engineering A 384 (1-2), (2004), 143-150.

[55] J. C. Ion, Laser Processing of Engineering Materials: Principles, Procedure and Industrial Application, Elsevier Butterworth-Heinemann, Oxford, 2005, p.219.

[56] K.W. Ng, H.C. Man, T.M. Yue, Characterization and corrosion study of NiTi laser surface alloyed with Nb and Co, Applied Surface Science 257 (2011) 3269-3274.

[57] F. Gao, H.M. Wang, Dry sliding wear property of a laser melting/deposited Ti_2Ni/TiNi intermetallic alloy, Intermetallics 16 (2008) 202-208.

[58] F. Gao, H.M. Wang, Effect of TiNi in dry sliding wear of laser melt deposited Ti_2Ni/TiNi alloys, Materials Characterization 59 (2008) 1349-1354.

[59] F. Gao, H.M. Wang, Abrasive wear property of laser melting/deposited Ti_2Ni/TiNi intermetallic alloy, Transactions of Nonferrous Metals Society of China 17 (2007) 1358-1362.

[60] N. Figueira, T.M. Silva, M.J. Carmezim, J.C.S. Fernandes, Corrosion behavior of NiTi alloy, Electrochimica Acta 54 (2009) 921-926.

[61] S.H. Chang, W.C. Chiu, Selective leaching and surface properties of Ti50Ni50-xCux (x=0-20at.%) shape memory alloys for biomedical applications, Applied Surface Science 324 (2015) 106-113.

[62] X. Wen, N. Zhang, X. Li, Z. Cao, Electrochemical and histomorphometric evaluation of the TiNiCu shape memory alloy, Bio-Medical Materials and Engineering 7 (1997) 1-11.

[63] K.M. Ismail, A.M. Fathi, W.A. Badawy, Electrochemical behavior of copper-nickel alloys in acidic chloride solutions, Corrosion Science 48 (2006) 1912-1925.

[64] M. Pourbaix, Atlas of Electrochemical Equilibria in Aqueous Solutions, 2nd ed.,

NACE, Houston, 1974.

[65] M.R. Bateni, F. Asrafizadeh, J.A. Szpunar, R.A.L. Drew, Improving the tribological behavior of copper through novel Ti-Cu intermetallics coatings, Wear 253 (2002) 626-639.

[66] T. Sasada, S. Ban, S. Norose, T. Nakano, Wear of binary alloys – difference in wear mode between solid solutions and intermetallic compounds, Wear 159(2), (1992), 191-199.

[67] S. Jacobson, S. Hogmark, Surface modifications in tribological contacts, Wear, 266(3-4), (2009), 370-378.

[68] W. Yan, Theoretical investigation of wear-resistance mechanism of superelastic shape memory alloy NiTi, Materials Science and Engineering A 427 (2006) 348-355.

[69] H Rösner, P Schloßmacher, A.V Shelyakov, A.M Glezer, Formation of TiCu plate-like precipitates in Ti50Ni25Cu25 shape memory alloys, Scripta Materialia (2000) 871-876.

[70] P. Gargarella, S. Pauly, K.K. Kong, J. Hu, N.S. Barekar, M. Samidi Khoshkhoo, A. Teresiak, H. Wendrock, U. Kuhn, C. Ruffing, E. Kerscher, J. Eckert, Ti-Cu-Ni shape memory bulk metallic glass composites, Acta Materialia 61 (2013) 151-162.

[71] L. Yan, Y. Lin, E. Liu, Wear behavior of martensitic NiTi shape memory alloy under ball-on-disk sliding tests, Tribology International 66 (2013) 219-224.

[72] Y. Liu, Z. Xie, J. Van Humbeeck, L. Delaey, Deformation of shape memory alloys associated with twinned domain re-configurations, Materials Science and Engineering A273-275 (1999) 679-684.

[73] Y. Liu, Z. Xie, J. Van Humbeeck, L. Delaey, Some results of the detwinning process in NiTi shape memory alloys, Scripta Materialia (1999) 1273-1281.

[74] S. Jiang, Y. Zhao, Y. Zhang, L. Hu, Y. Liang, Effect of solution treatment and aging on microstructural evolution and mechanical behavior of NiTi shape memory alloy, Transactions of Nonferrous Metals Society of China 23 (2013) 3658-3667.

[75] K. Gall, K. Juntunen, H.J. Maier, H. Sehitoglu, Y.I. Chumlyakov, Instrumented micro-indentation of NiTi shape memory alloys, Acta Materialia 49 (2001) 3205-3217.

[76] K. Gall, H.J. Maier, Cyclic deformation mechanisms in precipitated NiTi shape memory alloys, Acta Materialia 50 (2002) 4643-4657.

[77] J.I. Kim, S. Miyazaki, Effect of nano-scaled precipitates on shape memory behavior of Ti-50.9at.%Ni alloy, Acta Materialia 53 (2005) 4545-4554.

[78] D.Y. Li, Development of novel tribo composites with TiNi shape memory alloy matrix, Wear 255 (2003) 617-628.

[79] N.P. Suh, Tribophysics, Prentice-Hall, Englewood Cliffs, NJ, 1986.

[80] Paulmier, D., Bouchoucha, A., & Zaidi, H. (1990). Influence of the electrical current on wear in a sliding contact copper chrome steel, and connection with the environment. Vacuum, 41(7-9), 2213-2216.

[81] M. Abedini, H. M. Ghasemi & M. Nili Ahmadabadi Self-healing effect on worn surface of NiTi shape memory alloy, Materials Science and Technology, 26 (2010) 285-288.

[82] B. Shangguan, Y. Z. Zhang, J. D. Xing, L. M. Sun, Y. Chen, Study on the friction and wear of electrified copper against copper alloy under dry or moist conditions, Tribology Transactions 53 (2010) 927-932.

[83] K.W. Ng, H.C. Man, F.T. Cheng, T.M. Yue, Laser cladding of copper with molybdenum for wear resistance enhancement in electrical contacts, Appl. Surf. Sci. 253 (2007) 6236-6241.

[84] J.P. Tu, W. Rong, S.Y. Guo, Y.Z. Yang, Dry sliding wear behavior of in situ Cu-TiB_2 nanocomposites against medium carbon steel, Wear 255 (2003) 832-835.

Sample	Thickness of alloyed layer *D* (mm)	No. of layers	Laser processing parameters					
			Power (kW)	Spot size (mm)	Scanning speed for the layer (mm/s)			Dilution ratio *DR* (%)
					1st	2nd	3rd	
LA-NiTi-Cu-25-25	0.85	2	2	2	25	25	–	65
LA-NiTi-Cu-35-35	0.65	2	2	2	35	35	–	54
LA-NiTi-Cu-35-45	0.53	2	2	2	35	45	–	43
LA-NiTi-Cu-35-45-45	0.60	3	2	2	35	45	45	25

Table 1. Laser processing parameters and sample designations.

Sample	Average content (at.%)				Major phase	Minor phases
	O	Ti	Ni	Cu		
cp Cu	0	0	0	100	α-Cu	–
LA-NiTi-Cu-25-25	3	11	12	74	α-CuNiTi	NiTi (B19'), Ni_3Ti, CuTi, TiO_2/$NiTiO_3$
LA-NiTi-Cu-35-35	3	33	31	33	$(NiCu)_4Ti_3$	NiTi (B19'), Ni_3Ti, CuTi, TiO_2/$NiTiO_3$
LA-NiTi-Cu-35-45	7	35	34	24	$(NiCu)_4Ti_3$	NiTi (B19'), Ni_3Ti, CuTi, TiO_2/$NiTiO_3$
LA-NiTi-Cu-35-45-45	5	39	38	18	NiTiCu (B19')	Ni_4Ti_3, Ni_3Ti, CuTi, TiO_2/$NiTiO_3$
NiTi plate	0	50	50	0	NiTi (B19')	–

Table 2. Overall compositions, phases present and *ICR* values of cp Cu, laser-alloyed samples and NiTi plate.

Sample	Phase (refer to Fig. 6)	O (at.%)	Ti (at.%)	Ni (at.%)	Cu (at.%)
LA-NiTi-Cu-25-25	White	2.2	3.3	5.0	89.5
	Grey	-	14.6	17.4	68.0
	Black	21.2	24.8	11.5	42.5
LA-NiTi-Cu-35-35	White	-	11.4	13.8	74.8
	Grey	-	19.3	21.7	59.0
	Black	43.4	35.1	4.6	16.9
LA-NiTi-Cu-35-45	White	3.3	19.4	17.8	59.5
	Grey	-	30.8	34.5	34.7
	Black	20.1	45.2	17.2	17.5
LA-NiTi-Cu-35-45-45	White	3.7	37.5	42.1	16.7
	Grey	-	41.1	45.7	13.2
	Black	6.7	45. 5	34.9	12.9

Table 3. Compositions of various phases present in the laser-alloyed samples.

Sample	Average hardness ($HV_{0.2}$)	Elastic recovery ratio %	Susceptibility to cracking in air		Susceptibility to cracking in SAR		*OCP* (V_{SCE})	I_{corr} ($\mu A/cm^2$)	*ICR* ($m\Omega \cdot cm^2$) at 50 N/cm^2
			Surface	Internal	Surface	Internal			
cp Cu	75 ± 2	7.5 ± 0.4	No	No	No	No	-0.055	1.570	0.031
NiTi plate	346 ± 18	42.0 ± 1.3	-	-	-	-	-0.111	0.022	-
LA-NiTi-Cu-25-25	240 ± 11	19.0 ± 0.6	Yes	No	No	No	0.025	1.479	0.109
LA-NiTi-Cu-35-35	455 ± 17	25.3 ± 0.7	Yes	No	No	No	0.022	0.635	0.149
LA-NiTi-Cu-35-45	465 ± 22	26.9 ± 1.4	Yes	No	No	No	0.022	0.515	0.154
LA-NiTi-Cu-35-45-45	435 ± 43	29.6 ± 1.4	Yes	No	No	No	-0.030	0.219	0.223
LA-W-Cu-p2 [39]	150 ± 26	-	Yes	Yes	Yes	Yes	-0.144	0.925	1.117
LA-Ti-Cu-20 [38]	661 ± 41	-	Yes	Yes	Yes	Yes	-0.082	0.697	0.158

Table 4. Average hardness, elastic recovery ratio, corrosion parameters in SAR (open to air) at 25 ^{o}C, and ICR of various laser-alloyed samples, cp Cu and NiTi plate.

Sample	Wear rate (mm/h)					*E/T* %	*S/T* %	*C/T*% 10^{-6}
	Dry	*E* (in DW)	*T* (in SAR)	*C* (in SAR) 10^{-6}	*S*			
cp Cu	293	223	270	4.16	36.8	85.8	14.2	1.60
LA-NiTi-Cu-25-25	0.13	0.04	0.06	3.62	0.02	63.9	36.1	5934
LA-NiTi-Cu-35-35	0.12	0.03	0.04	1.20	0.01	70.0	30.0	3000
LA-NiTi-Cu-35-45	0.11	0.03	0.04	0.99	0.01	65.0	35.0	2465
LA-NiTi-Cu-35-45-45	0.08	0.02	0.03	0.37	0.01	70.6	29.4	1088
LA-W-Cu-p2 [40]	1.16	0.50	0.65	1.18	0.15	76.9	23.1	209
LA-Ti-Cu-30 [38]	1.56	1.13	1.18	1.63	0.05	95.8	4.2	138

Table 5. Wear rates of cp Cu and laser-alloyed samples after wear test for 1 km and 20-60 km respectively in 60 km/h, 60 A in various environments.

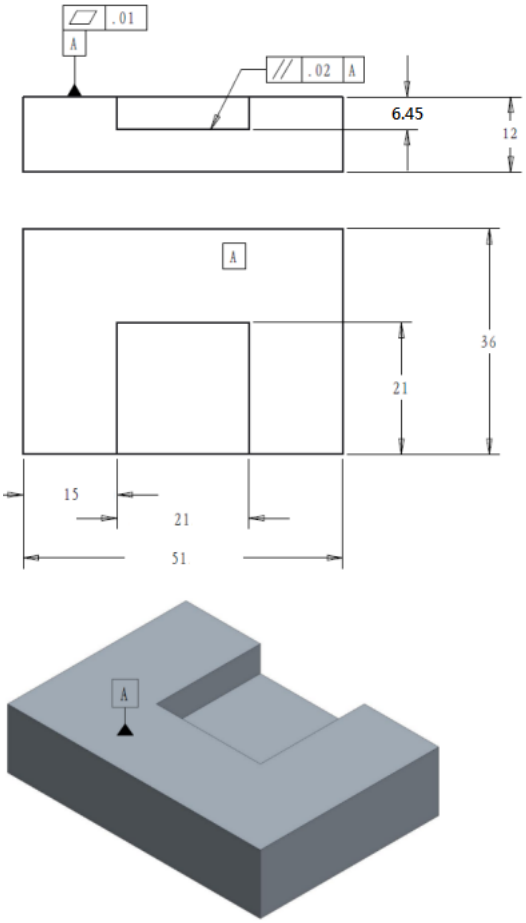

(a)

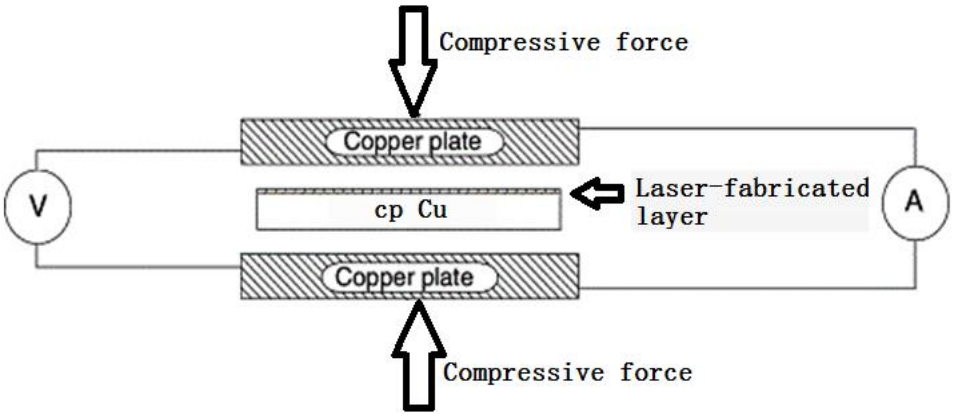

(b)

Fig. 1. Fixture for preplacing the coatings (all dimensions are in mm); and (b) Schematic diagram of interfacial contact resistance (*ICR*) measurement.

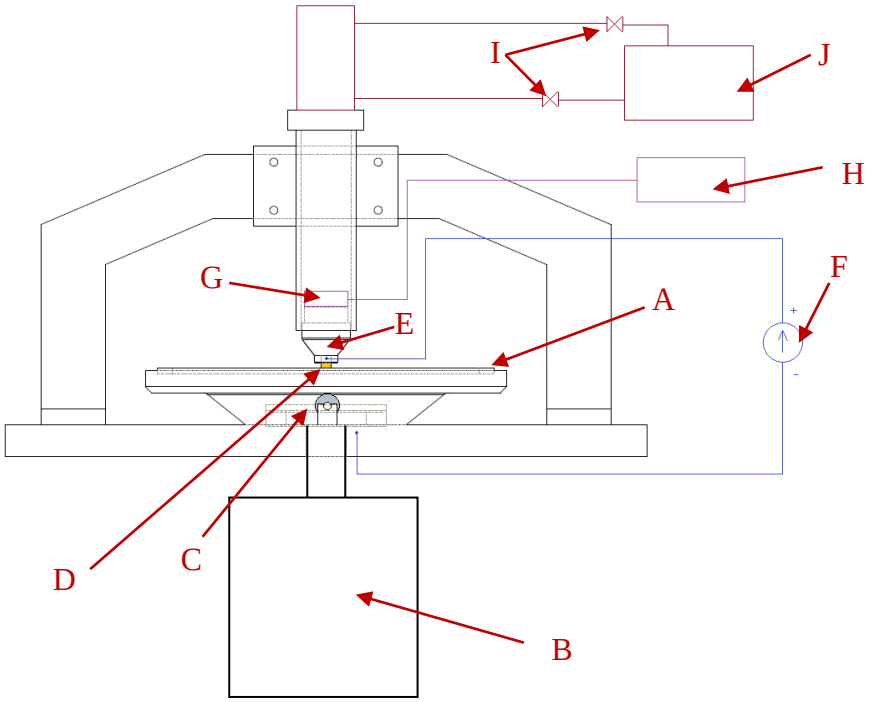

Fig. 2. Schematic diagram of pin-on-disc tribometer: (A) rotating disc; (B) high speed motor; (C) bearing support; (D) specimen; (E) specimen holder; (F) power supply; (G) force sensor; (H) manometer; (I) oil control valves; (J) oil pressure pump and tank.

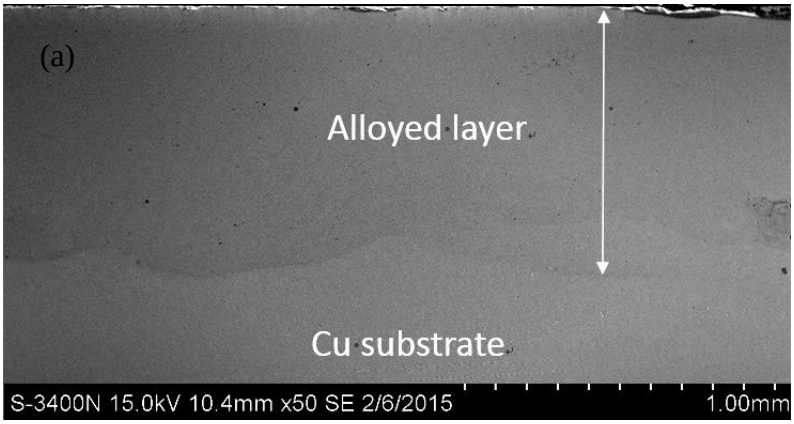
(a)
Alloyed layer
Cu substrate
S-3400N 15.0kV 10.4mm x50 SE 2/6/2015
1.00mm

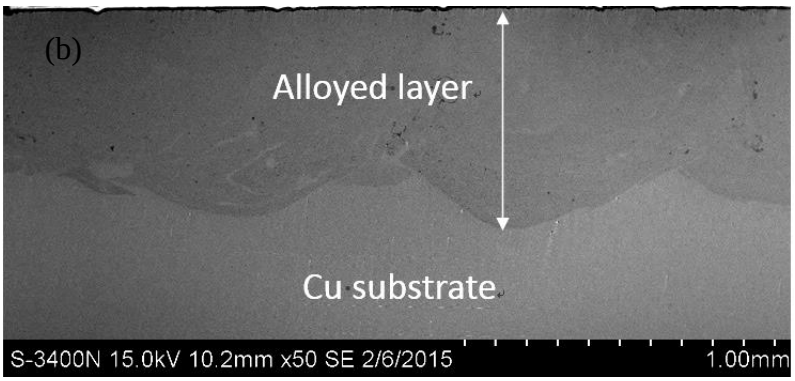
(b)
Alloyed layer
Cu substrate
S-3400N 15.0kV 10.2mm x50 SE 2/6/2015
1.00mm

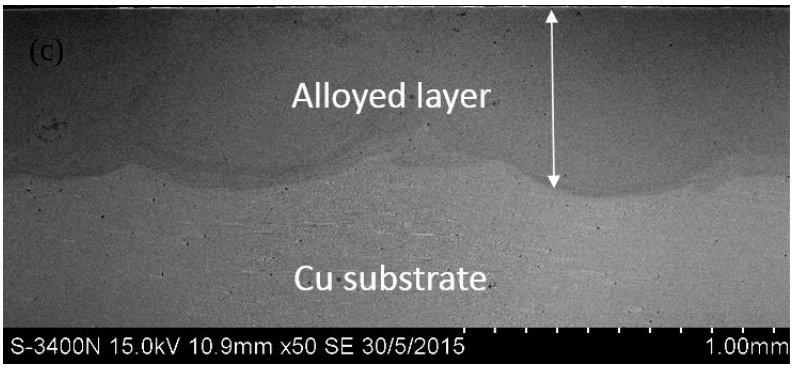
(c)
Alloyed layer
Cu substrate
S-3400N 15.0kV 10.9mm x50 SE 30/5/2015
1.00mm

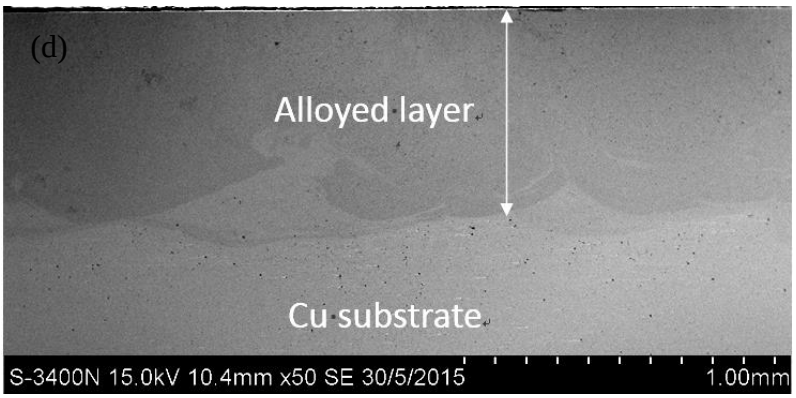
(d)
Alloyed layer
Cu substrate
S-3400N 15.0kV 10.4mm x50 SE 30/5/2015
1.00mm

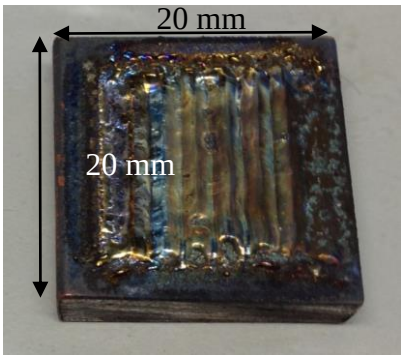

Fig. 3. Cross-sectional views of laser-alloyed samples: (a) LA-NiTi-Cu-25-25, (b) LA-NiTi-Cu-35-35, (c) LA-NiTi-Cu-35-45, (d) LA-NiTi-Cu-35-45-45 and (e) top view of LA-NiTi-Cu-35-45-45.

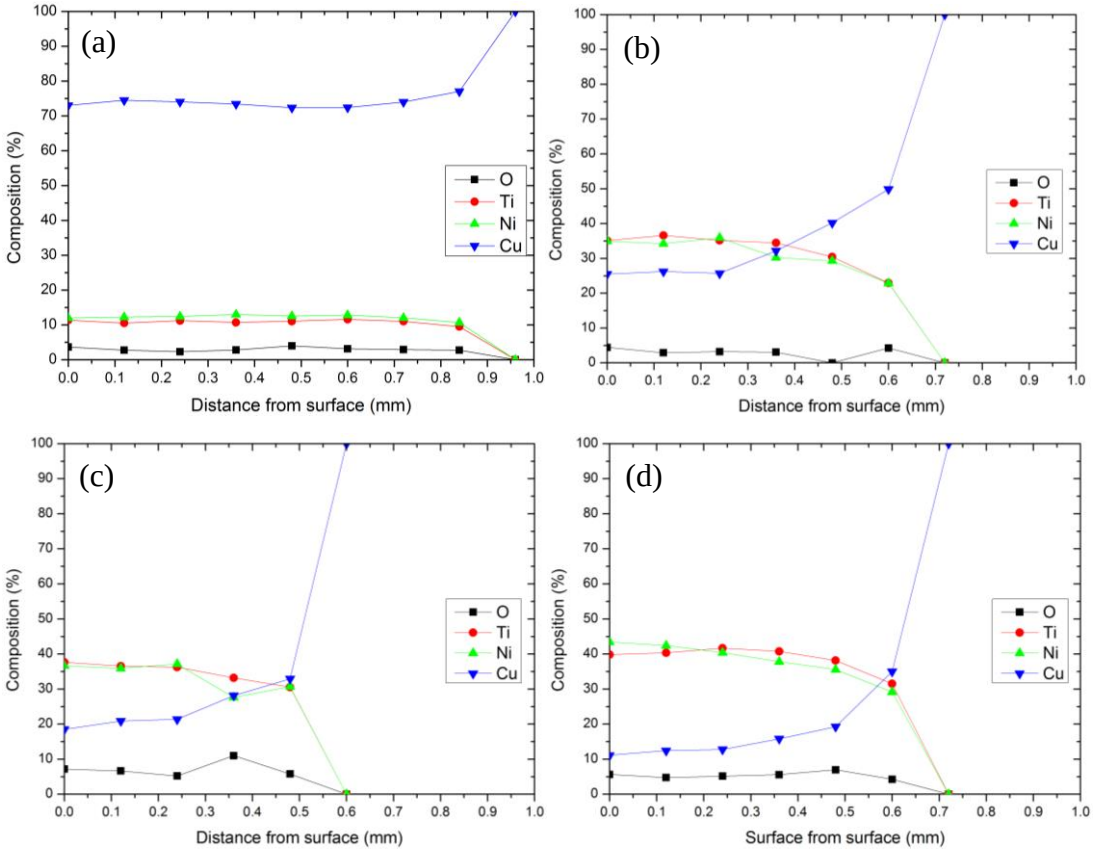

Fig. 4. Compositional profiles of laser-alloyed samples: (a) LA-NiTi-Cu-25-25, (b) LA-NiTi-Cu-35-35, (c) LA-NiTi-Cu-35-45 and (d) LA-NiTi-Cu-35-45-45.

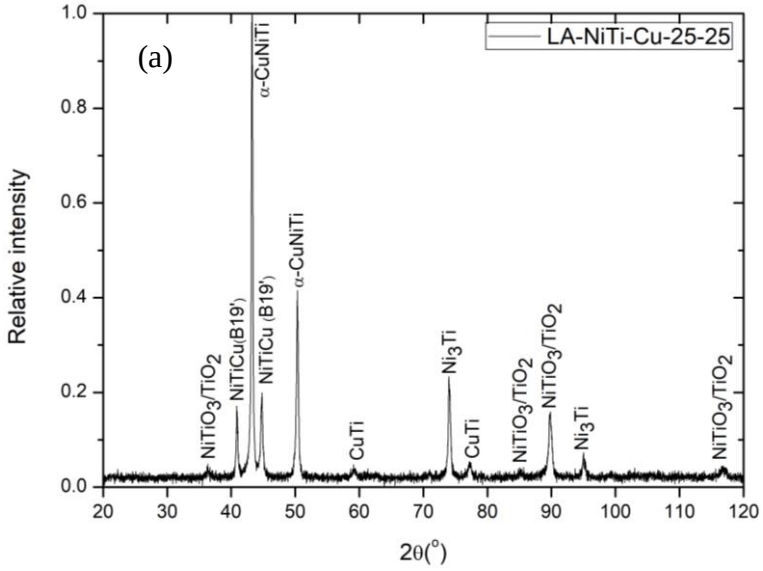
(a)
LA-NiTi-Cu-25-25
Relative intensity
2θ(°)
NiTiO3/TiO2
NiTiCu(B19')
α-CuNiTi
NiTiCu (B19')
α-CuNiTi
CuTi
Ni3Ti
CuTi
NiTiO3/TiO2
NiTiO3/TiO2
Ni3Ti
NiTiO3/TiO2

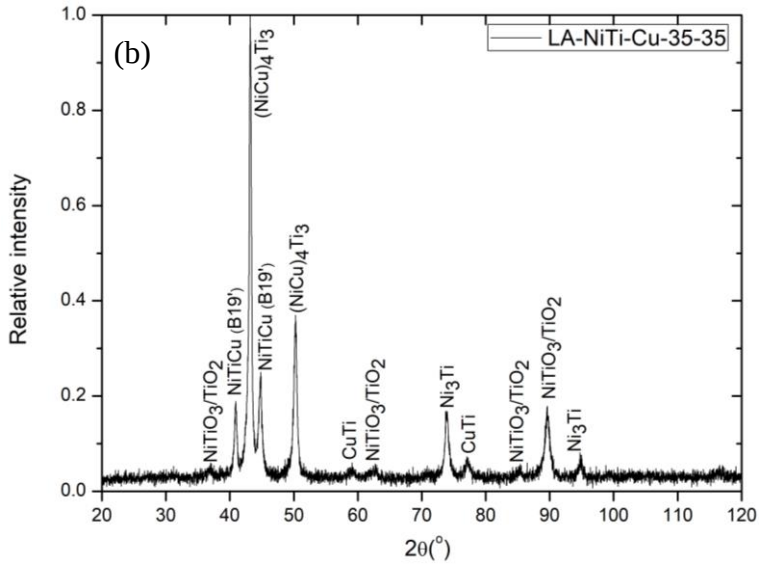
(b)
LA-NiTi-Cu-35-35
Relative intensity
2θ(°)
NiTiO3/TiO2
NiTiCu (B19')
(NiCu)4Ti3
NiTiCu (B19')
(NiCu)4Ti3
CuTi
NiTiO3/TiO2
Ni3Ti
CuTi
NiTiO3/TiO2
NiTiO3/TiO2
Ni3Ti

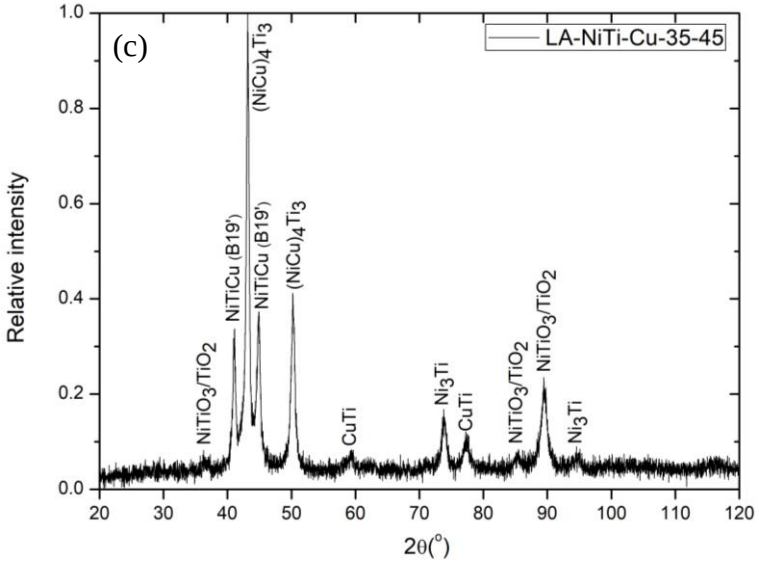
(c)
LA-NiTi-Cu-35-45
Relative intensity
2θ(°)
NiTiO3/TiO2
NiTiCu (B19')
(NiCu)4Ti3
NiTiCu (B19')
(NiCu)4Ti3
CuTi
Ni3Ti
CuTi
NiTiO3/TiO2
NiTiO3/TiO2
Ni3Ti

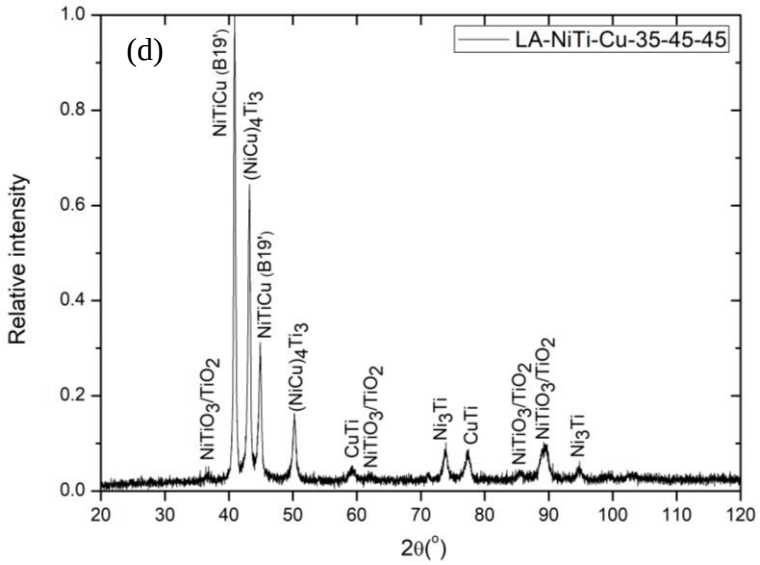

Fig. 5. XRD patterns of laser-alloyed samples: (a) LA-NiTi-Cu-25-25, (b) LA-NiTi-Cu-35-35, (c) LA-NiTi-Cu-35-45 and (d) LA-NiTi-Cu-35-45-45.

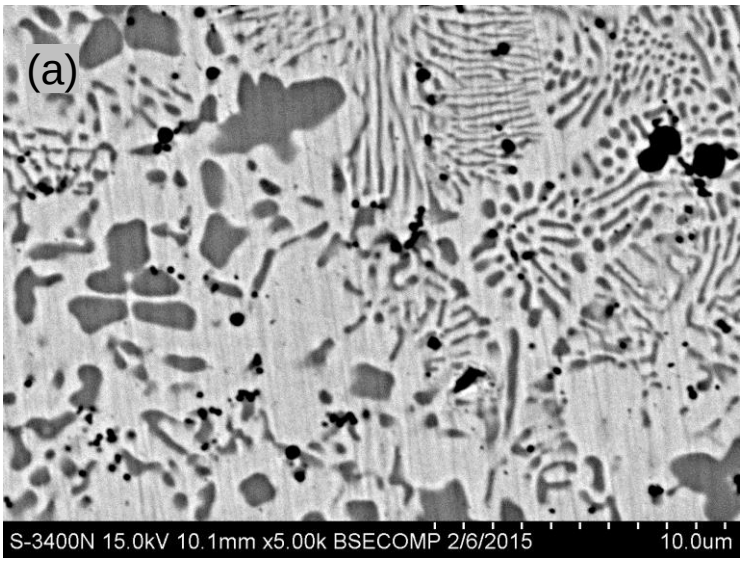
(a)
S-3400N 15.0kV 10.1mm x5.00k BSECOMP 2/6/2015
10.0um

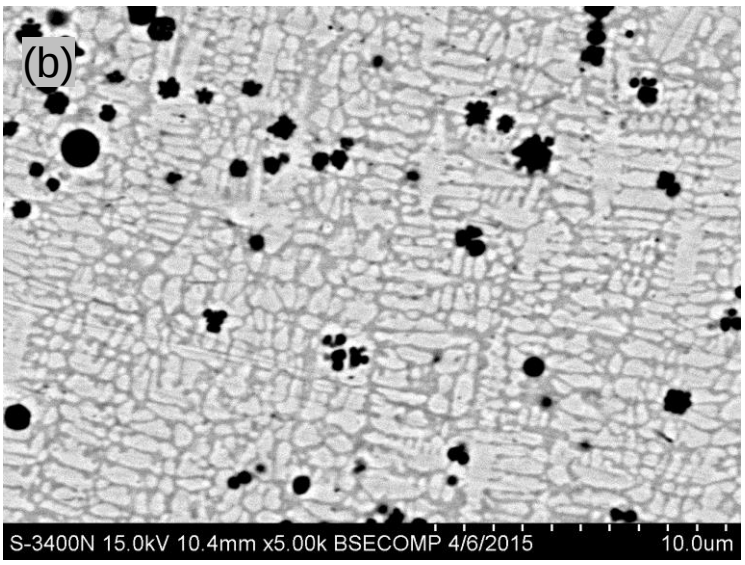
(b)
S-3400N 15.0kV 10.4mm x5.00k BSECOMP 4/6/2015
10.0um

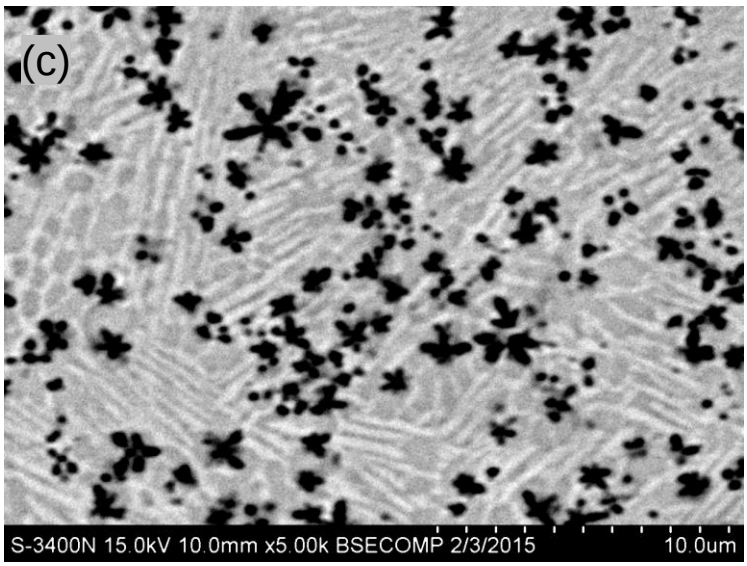
(c)
S-3400N 15.0kV 10.0mm x5.00k BSECOMP 2/3/2015
10.0um

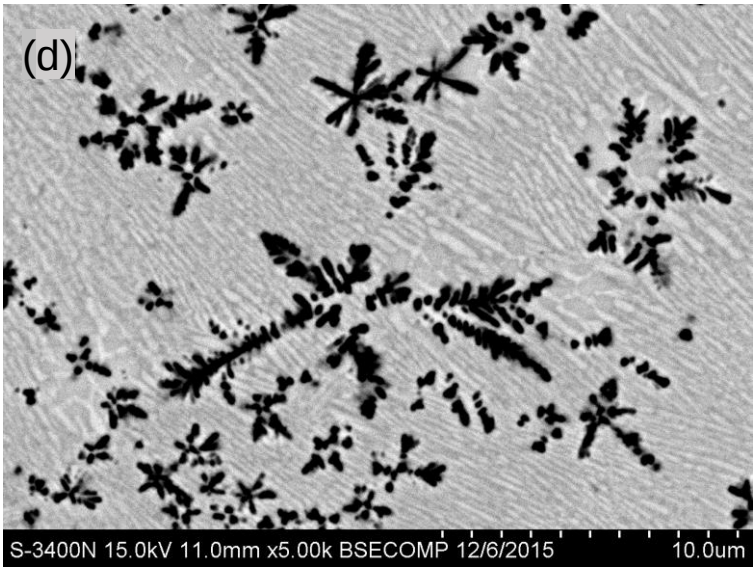

Fig. 6. Microstructure of laser-alloyed samples: (a) LA-NiTi-Cu-25-25, (b) LA-NiTi-Cu-35-35, (c) LA-NiTi-Cu-35-45 and (d) LA-NiTi-Cu-35-45-45.

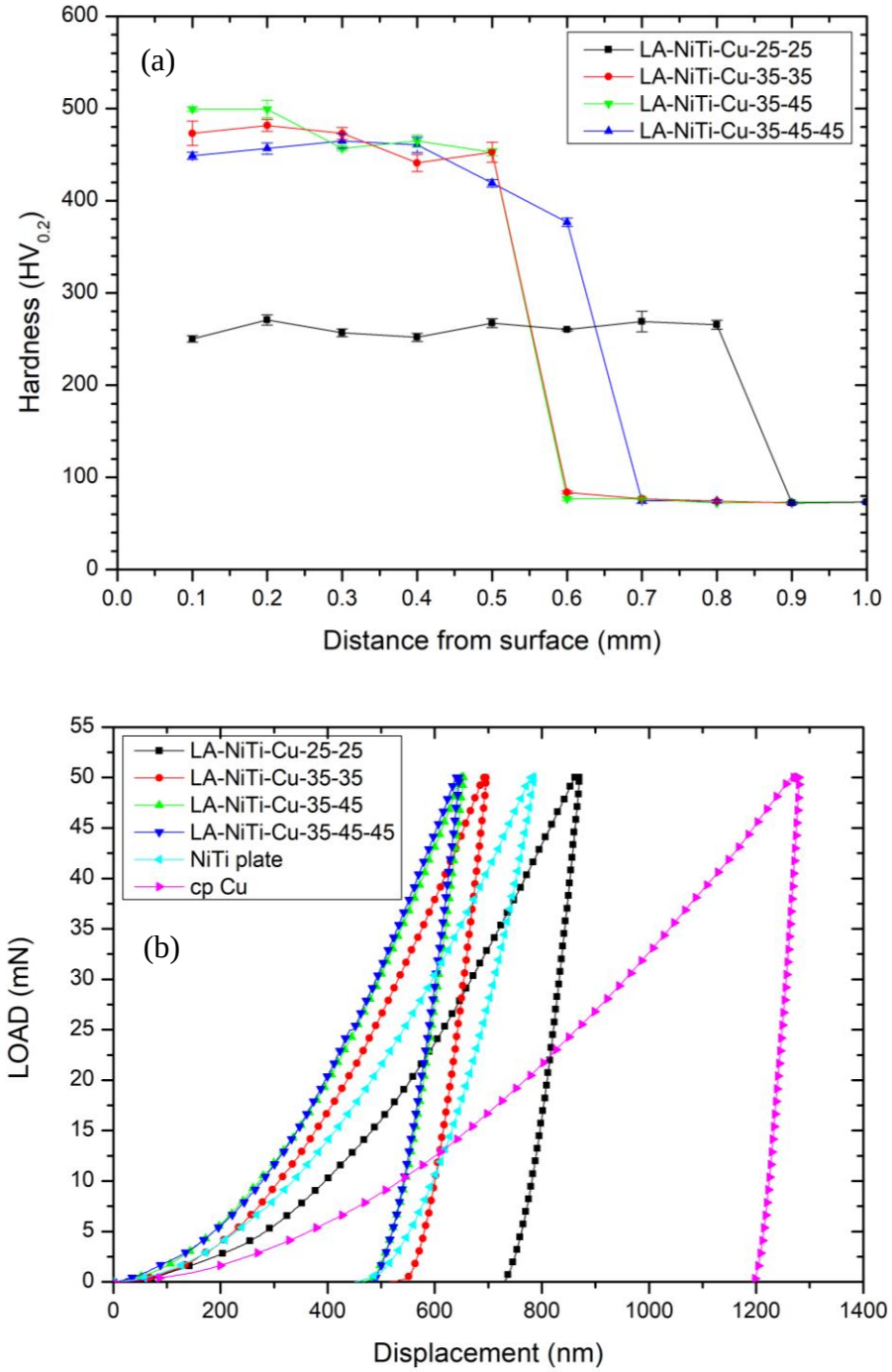

Fig. 7. (a) Hardness profiles and (b) nanoindentation curves of various laser-alloyed samples.

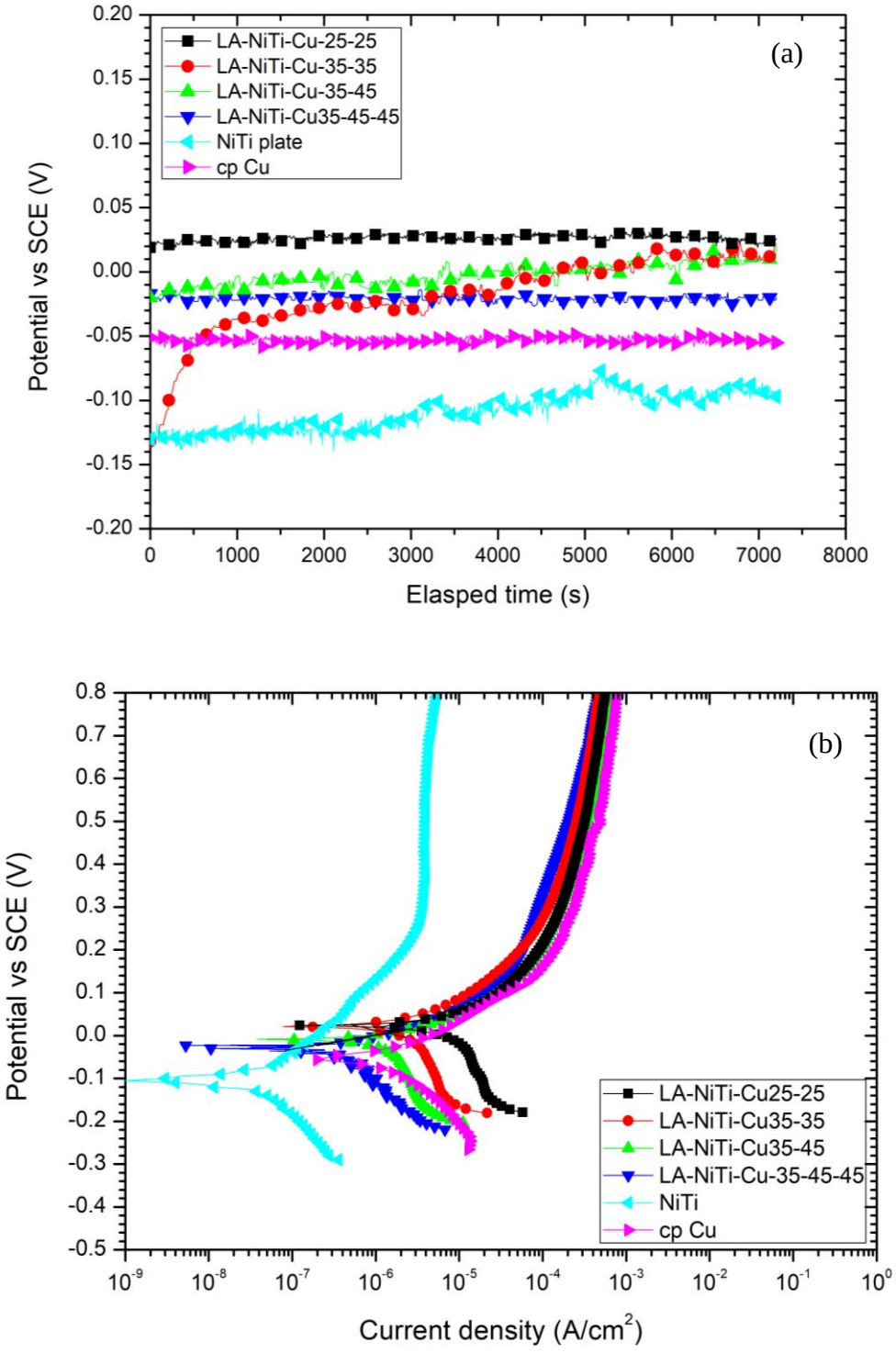

Fig. 8.(a) Plot of *OCP* vs time and (b) potentiodynamic polarization curves of various samples in SAR at 25 ^{o}C.

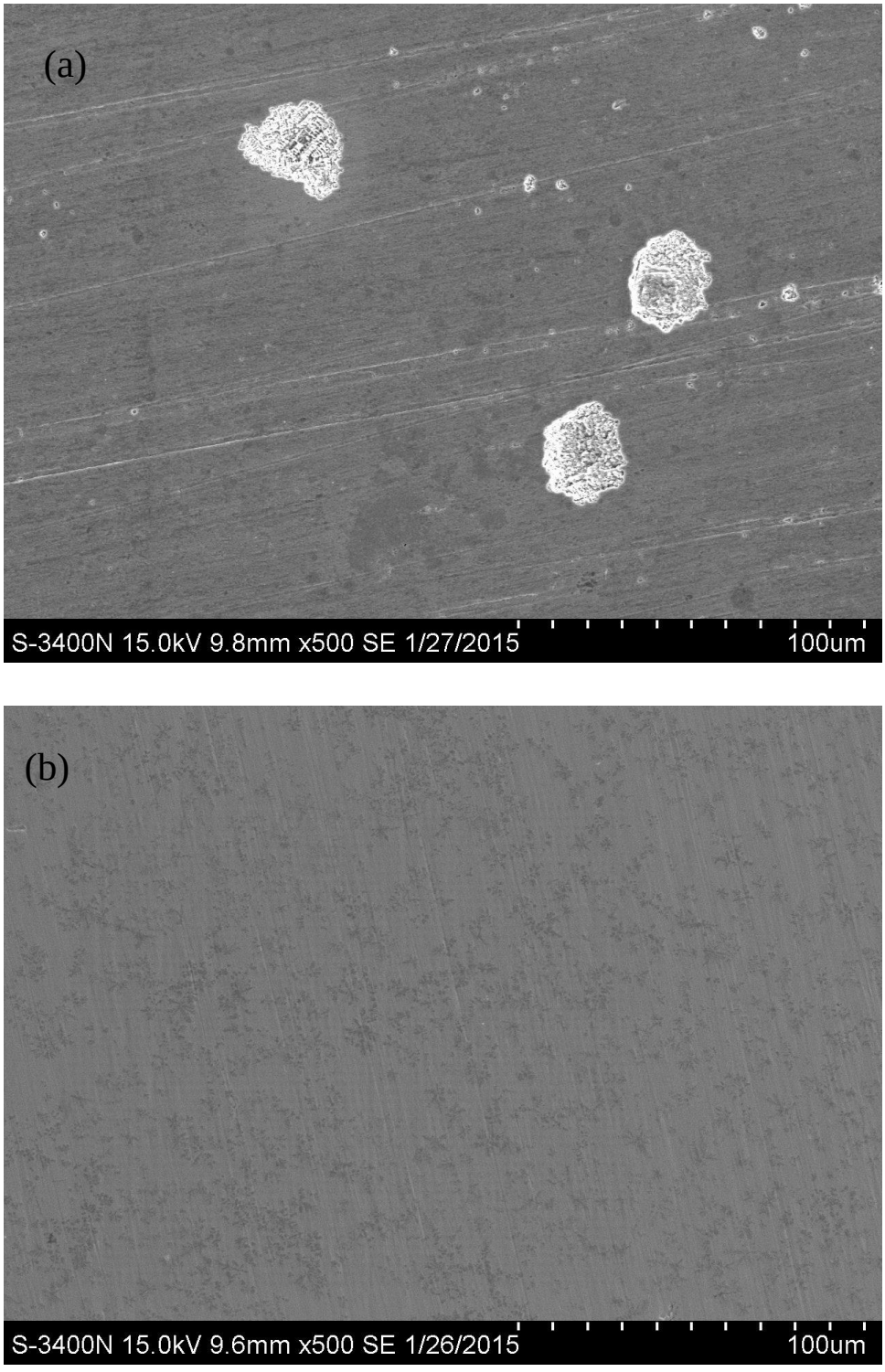

Fig. 9. SEM micrographs of corroded surfaces of (a) LA-NiTi-Cu-25-25 and (b) LA-NiTi-Cu-35-45-45 after potentiodynamic polarization test in SAR.

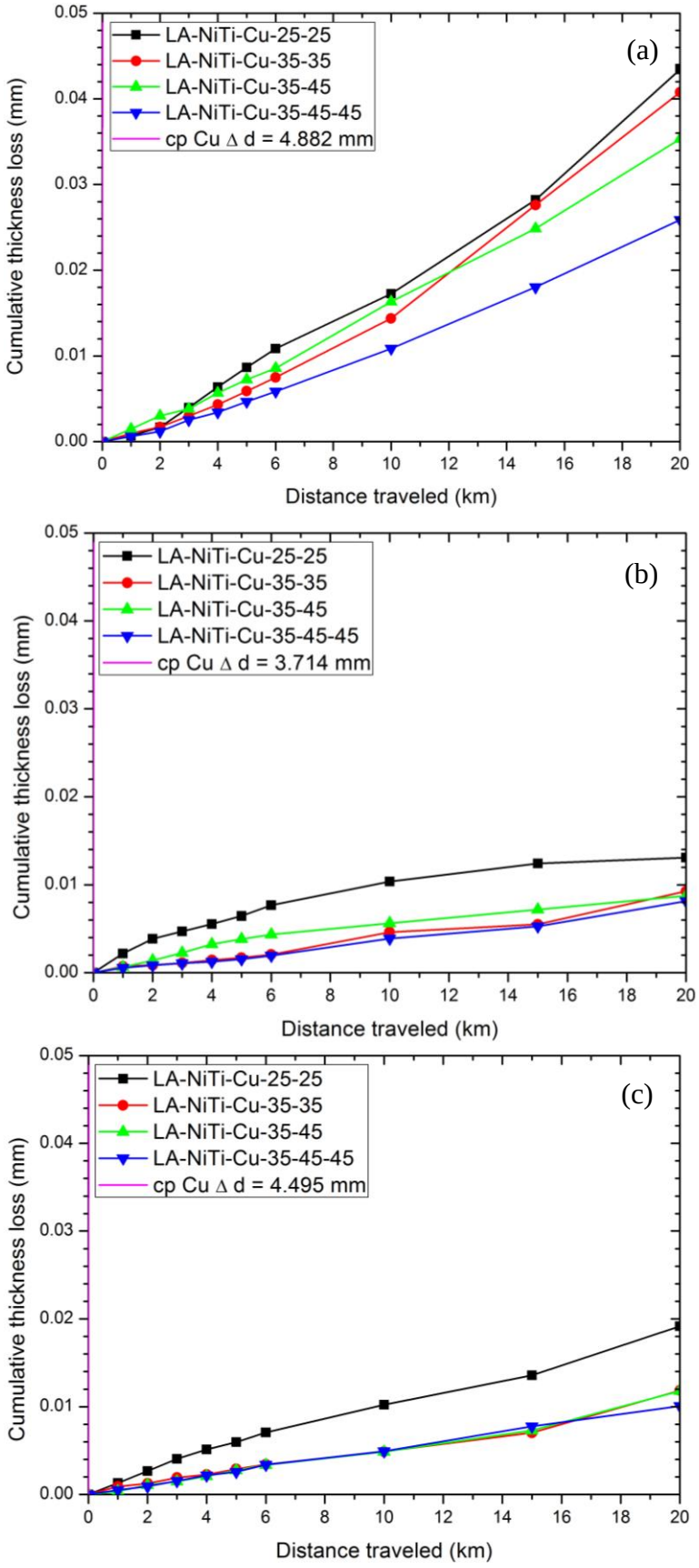

Fig. 10. Cumulative thickness loss against distance travelled for various samples in (a) dry wear (in air), (b) wet wear in DW and (c) wet wear in SAR at 60 km/h, 60 A.

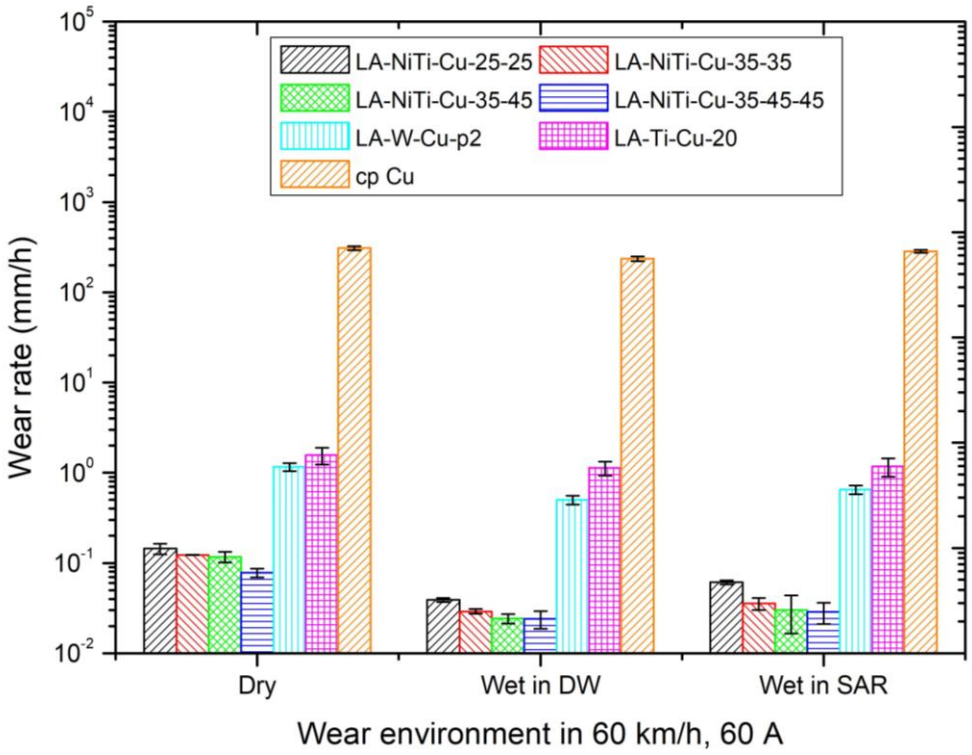

Fig. 11. Electrical sliding wear rate of various laser-alloyed samples and cp Cu in different wear environments at 60 km/h and 60 A [37, 39].

`

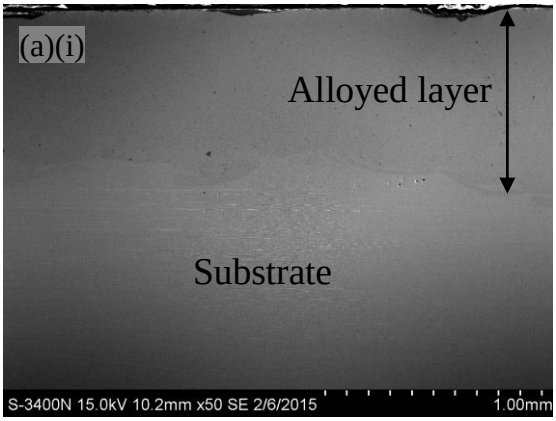

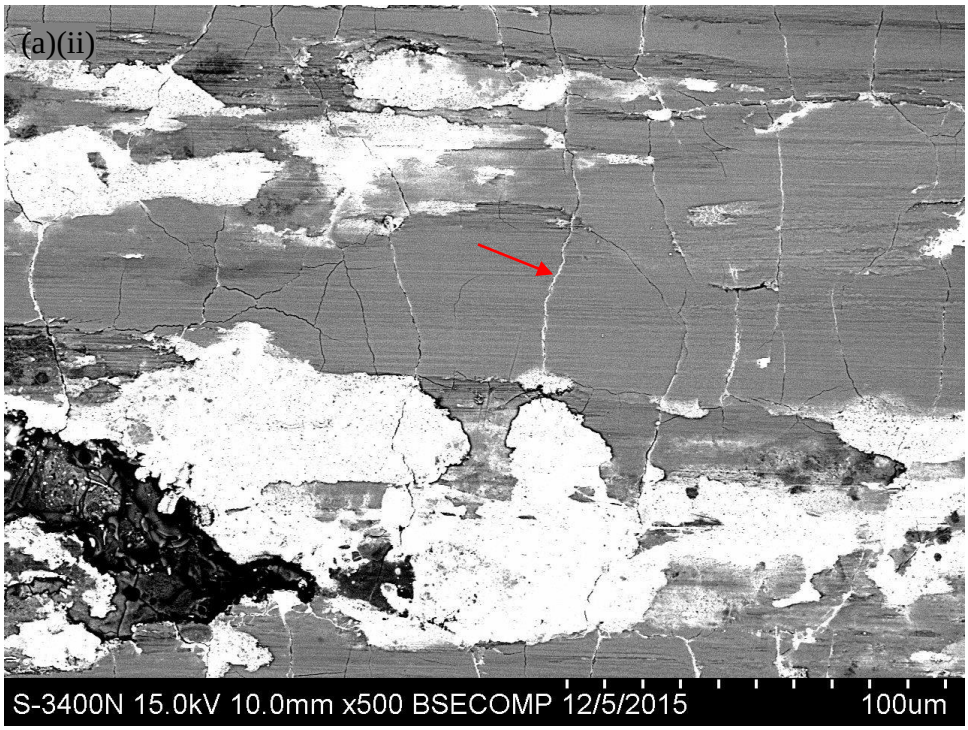

	O (at.%)	Ti (at.%)	Fe (at.%)	Ni (at.%)	Cu (at.%)	Hardness ($HV_{0.2}$)
Bright area	28.1	6.0	4.4	3.5	58.0	668 ± 26
Dark area	69.6	24.0	3.7	0.8	1.9	315 ± 36

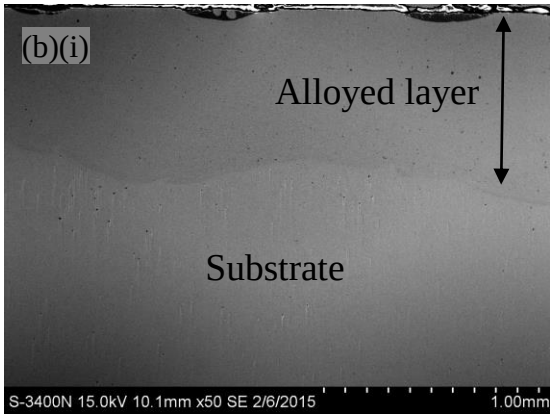

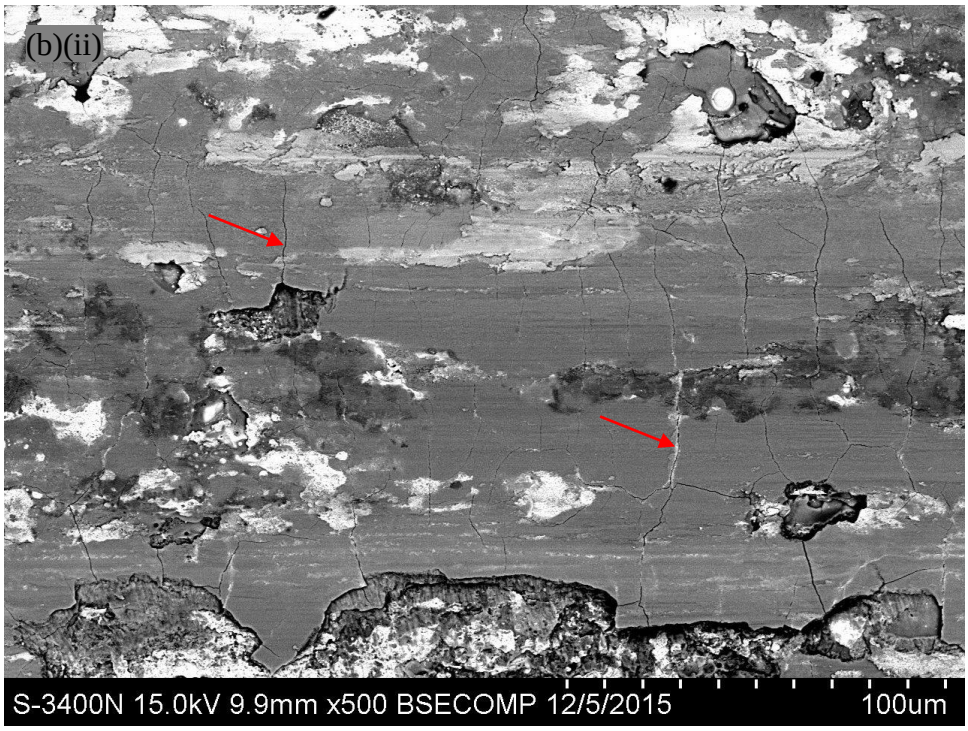

	O (at.%)	Ti (at.%)	Fe (at.%)	Ni (at.%)	Cu (at.%)	Hardness ($HV_{0.2}$)
Bright area	26.8	8.8	4.0	14.8	45.6	723 ± 55
Dark area	51.3	39.0	3.5	1. 8	4.4	615 ± 32

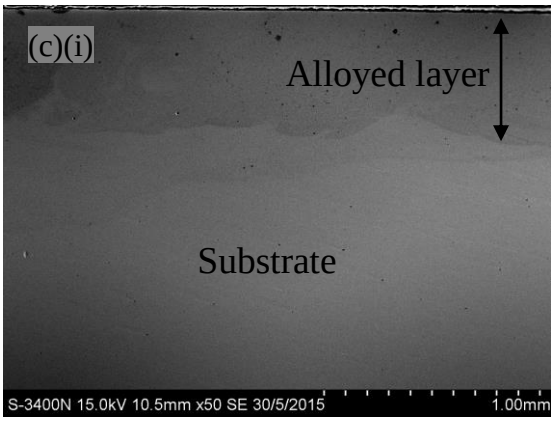

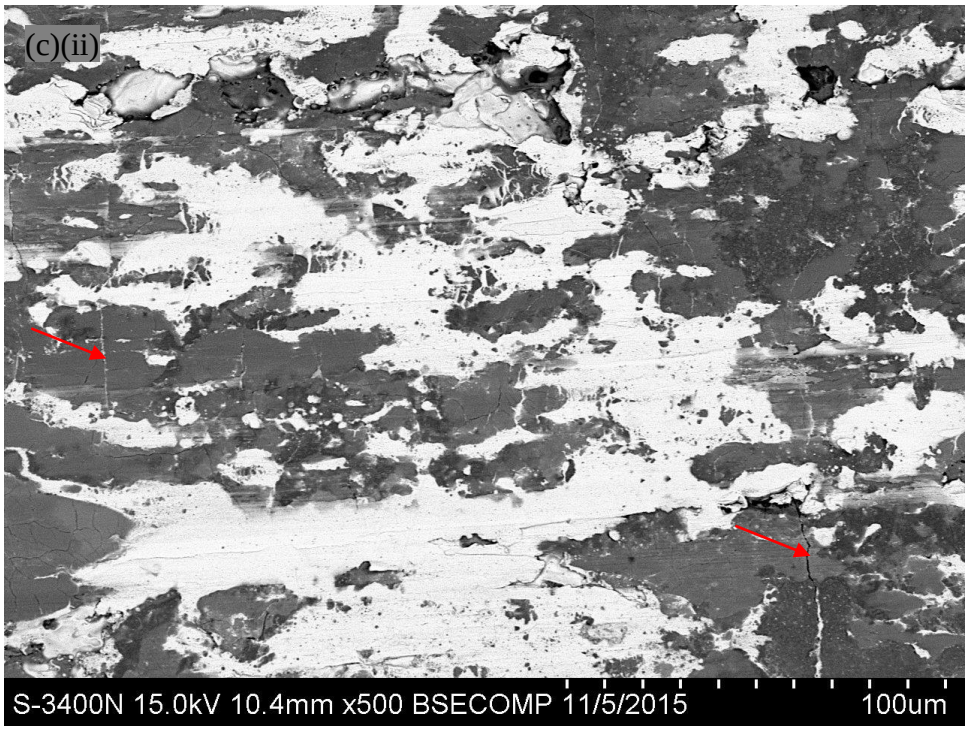

	O (at.%)	Ti (at.%)	Fe (at.%)	Ni (at.%)	Cu (at.%)	Hardness ($HV_{0.2}$)
Bright area	37.5	5.7	12.3	4.6	39. 8	780 ± 63
Dark area	65.7	18.2	8.8	1.9	5.4	631 ± 74

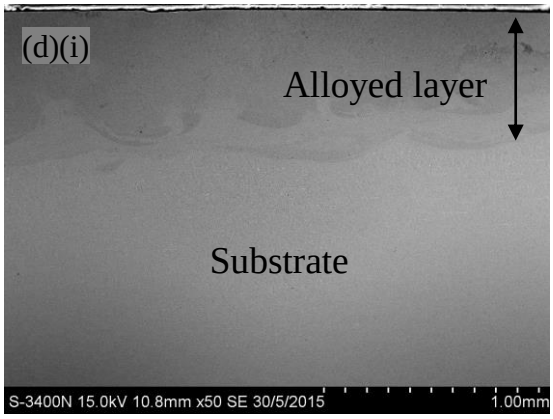

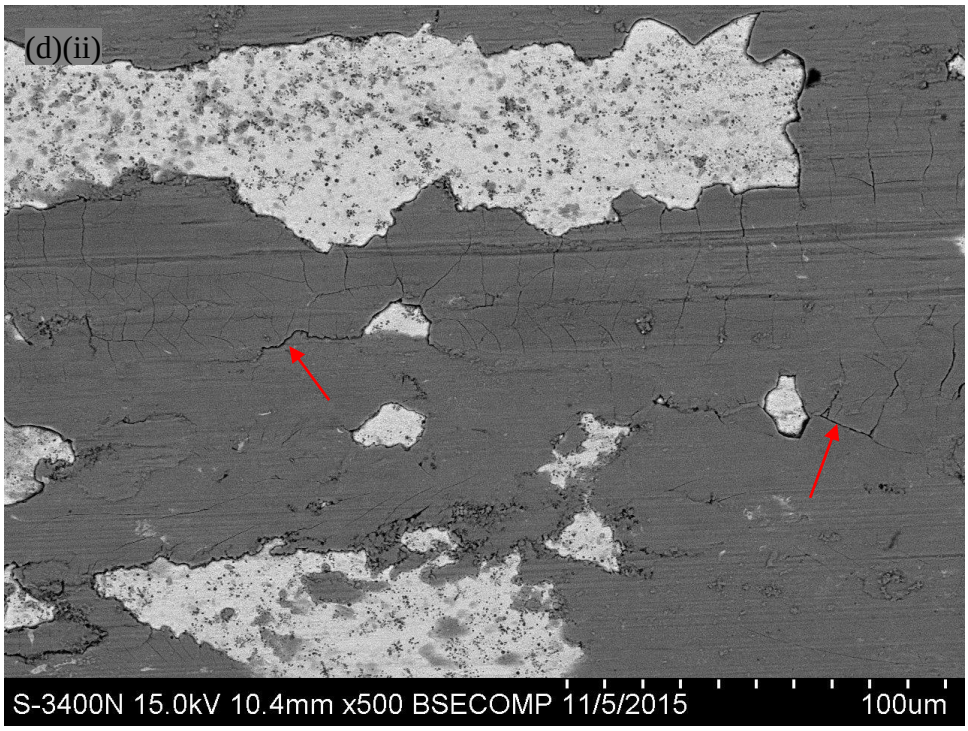

	O (at.%)	Ti (at.%)	Fe (at.%)	Ni (at.%)	Cu (at.%)	Hardness ($HV_{0.2}$)
Bright area	33.9	18.3	5.6	17.2	25.0	698 ± 63
Dark area	63.2	2.7	27.1	2.6	4.4	580 ± 21

Fig. 12. Worn surface of various samples in dry wear 60 km/h, 60 A: (a) LA-NiTi-Cu-25-25, (b) LA-NiTi-Cu-35-35, (c) LA-NiTi-Cu-35-45 and (d) LA-NiTi-Cu-35-45-45 (i) cross-sectional view of the alloyed layer; (ii) surface of the alloyed layer.

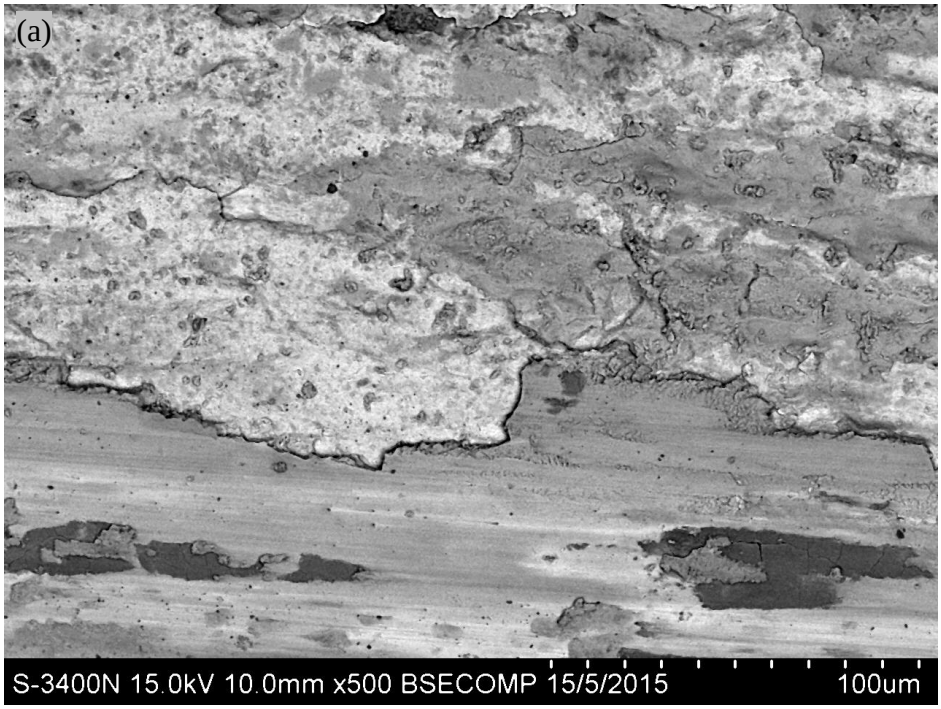

	O (at.%)	Ti (at.%)	Fe (at.%)	Ni (at.%)	Cu (at.%)	Hardness ($HV_{0.2}$)
Bright area	37.4	6.9	6.3	6.3	43.1	718 ± 90
Dark area	61.5	10.1	16.2	4.7	7.5	267 ± 52

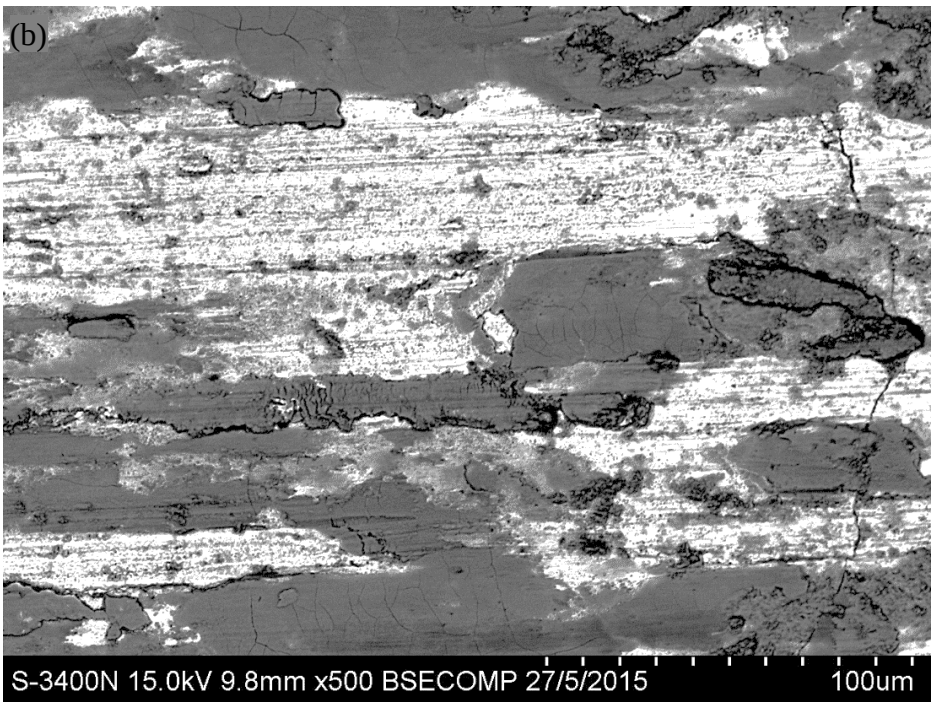

	O (at.%)	Ti (at.%)	Fe (at.%)	Ni (at.%)	Cu (at.%)	Hardness ($HV_{0.2}$)

Bright area	12.4	30.6	3.1	32.5	21.4	723 ± 45
Dark area	61.2	3.1	29.2	2.3	4.2	560 ± 58

(c)

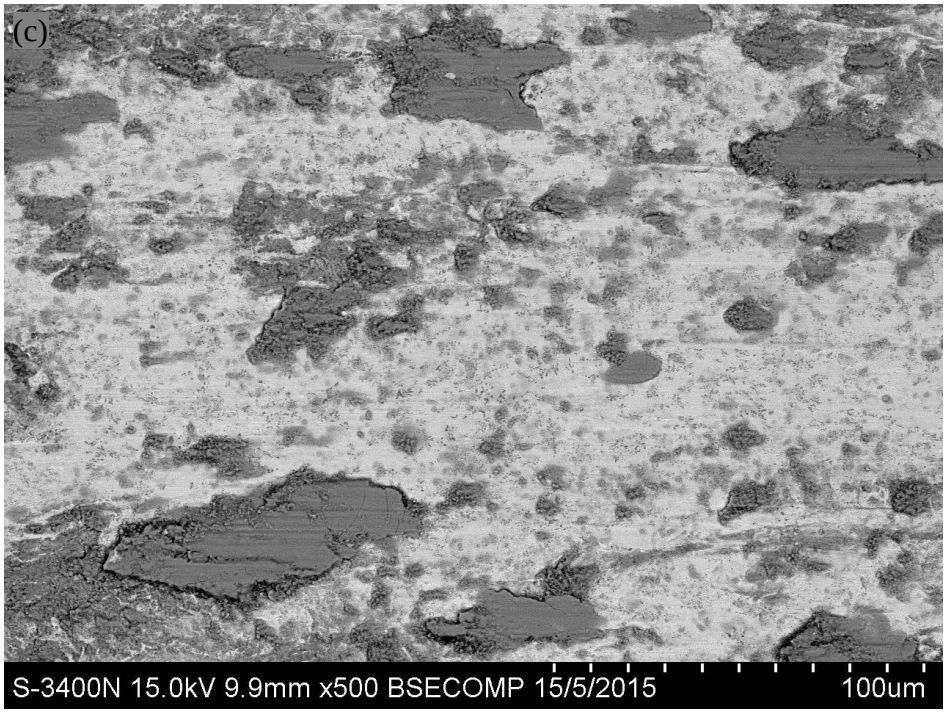

	O (at.%)	Ti (at.%)	Fe (at.%)	Ni (at.%)	Cu (at.%)	Hardness ($HV_{0.2}$)
Bright area	20.9	25.5	2.8	27.7	23.1	730 ± 58
Dark area	62.5	2.7	27.7	2.6	4.5	556 ± 36

(d)

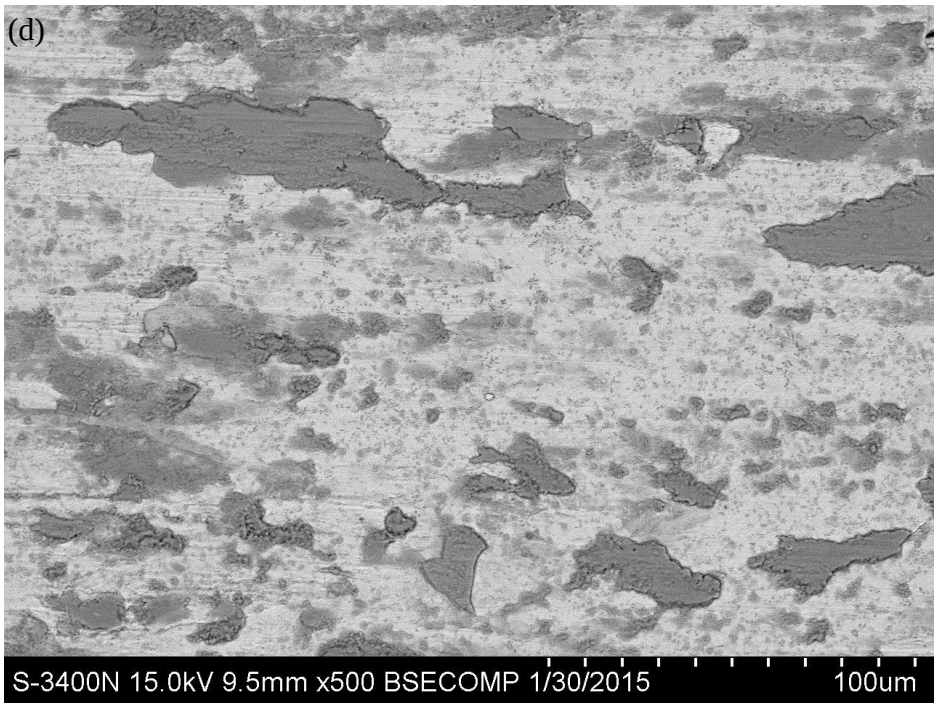

	O	Ti	Fe	Ni	Cu	Hardness

	(at.%)	(at.%)	(at.%)	(at.%)	(at.%)	($HV_{0.2}$)
Bright area	37.4	6.9	6.3	6.3	43.1	687 ± 94
Dark area	61.5	10.1	16.2	4.7	7.5	584 ± 12

Fig. 13. Worn surface of various samples in SAR wear 60 km/h, 60 A: (a) LA-NiTi-Cu-25-25, (b) LA-NiTi-Cu-35-35, (c) LA-NiTi-Cu-35-45 and (d) LA-NiTi-Cu-35-45-45.

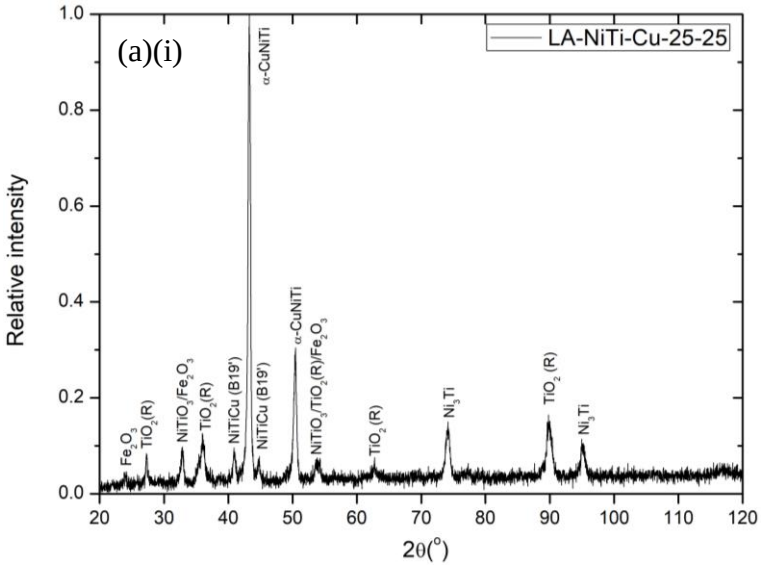
(a)(i)
LA-NiTi-Cu-25-25
Relative intensity
2θ(°)
α-CuNiTi
Fe2O3
TiO2(R)
NiTiO3/Fe2O3
TiO2(R)
NiTiCu (B19')
NiTiCu (B19')
α-CuNiTi
NiTiO3/TiO2(R)/Fe2O3
TiO2 (R)
Ni3Ti
TiO2 (R)
Ni3Ti

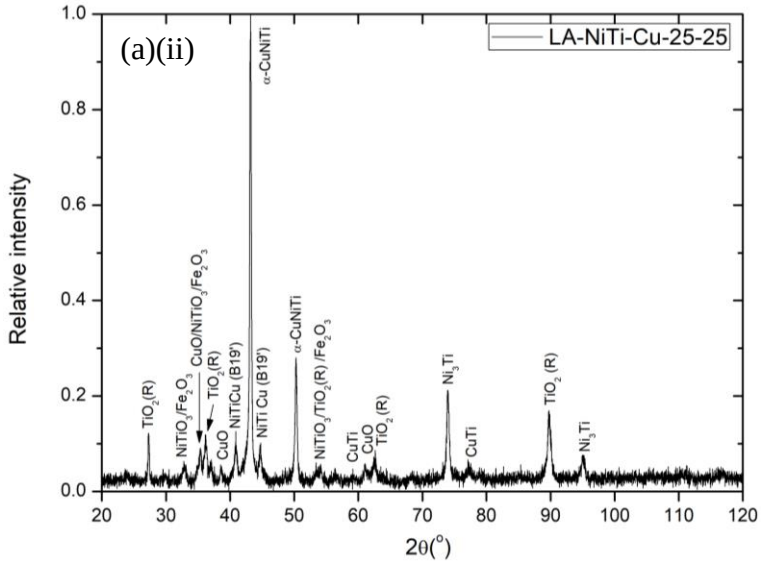
(a)(ii)
LA-NiTi-Cu-25-25
Relative intensity
2θ(°)
α-CuNiTi
TiO2(R)
NiTiO3/Fe2O3
CuO/NiTiO3/Fe2O3
TiO2(R)
CuO
NiTiCu (B19')
NiTi Cu (B19')
α-CuNiTi
NiTiO3/TiO2(R) /Fe2O3
CuTi
CuO
TiO2 (R)
Ni3Ti
CuTi
TiO2 (R)
Ni3Ti

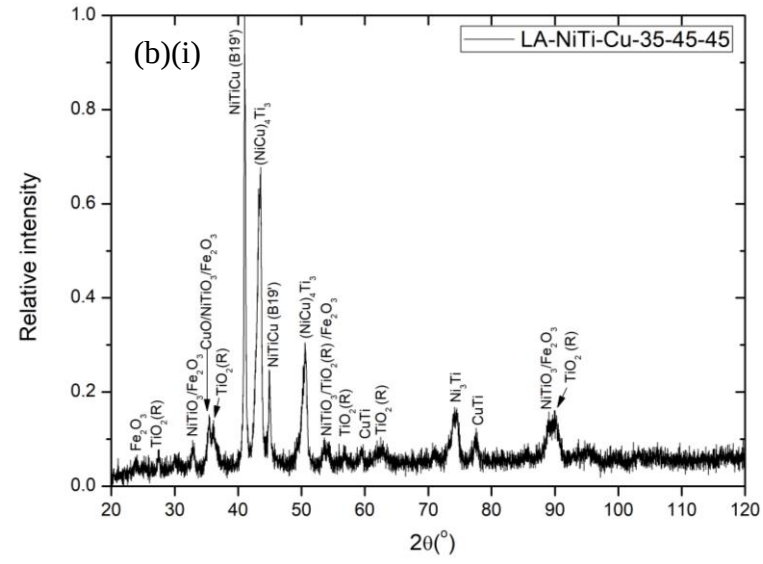
(b)(i)
LA-NiTi-Cu-35-45-45
Relative intensity
2θ(°)
NiTiCu (B19')
(NiCu)4Ti3
Fe2O3
TiO2(R)
NiTiO3/Fe2O3
CuO/NiTiO3/Fe2O3
TiO2(R)
NiTiCu (B19')
(NiCu)4Ti3
NiTiO3/TiO2(R) /Fe2O3
TiO2(R)
CuTi
TiO2 (R)
Ni3Ti
CuTi
NiTiO3/Fe2O3
TiO2 (R)

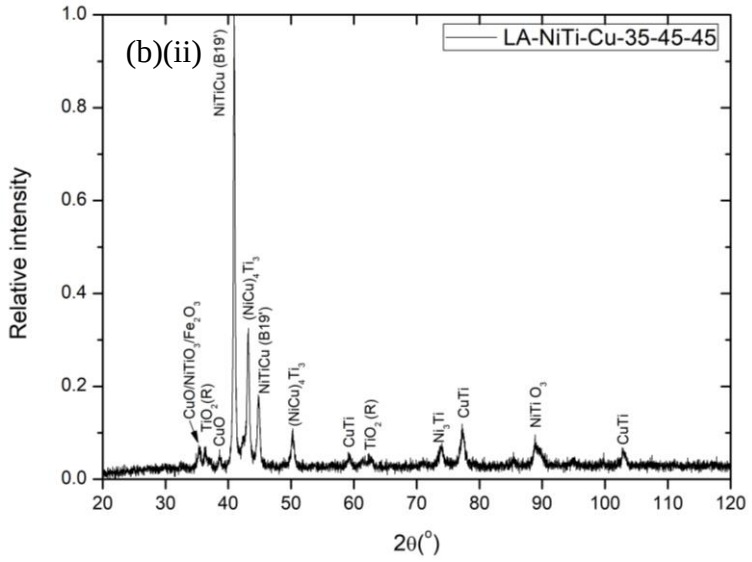

Fig. 14. XRD patterns of worn surface for (a) LA-NiTi-Cu-25-25 and (b) LA-NiTi-Cu-35-45-45 sliding at 60 km/h 60A in (i) dry condition and (ii) SAR solution.

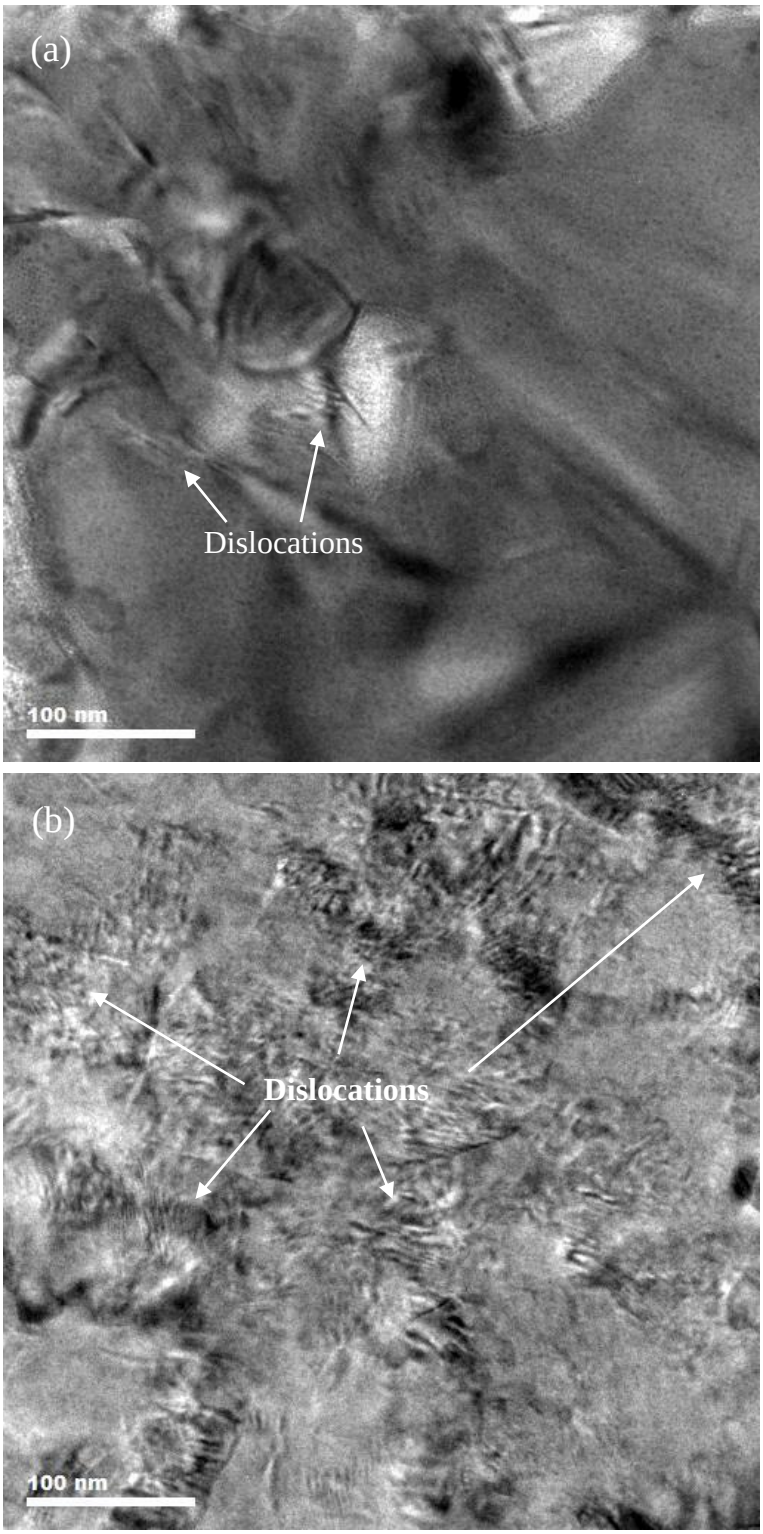

Fig. 15. TEM micrographs of LA-NiTi-Cu-35-45-45 (a) before and (b) after electrical sliding wear test at 60 km/h, 60A, in dry condition.

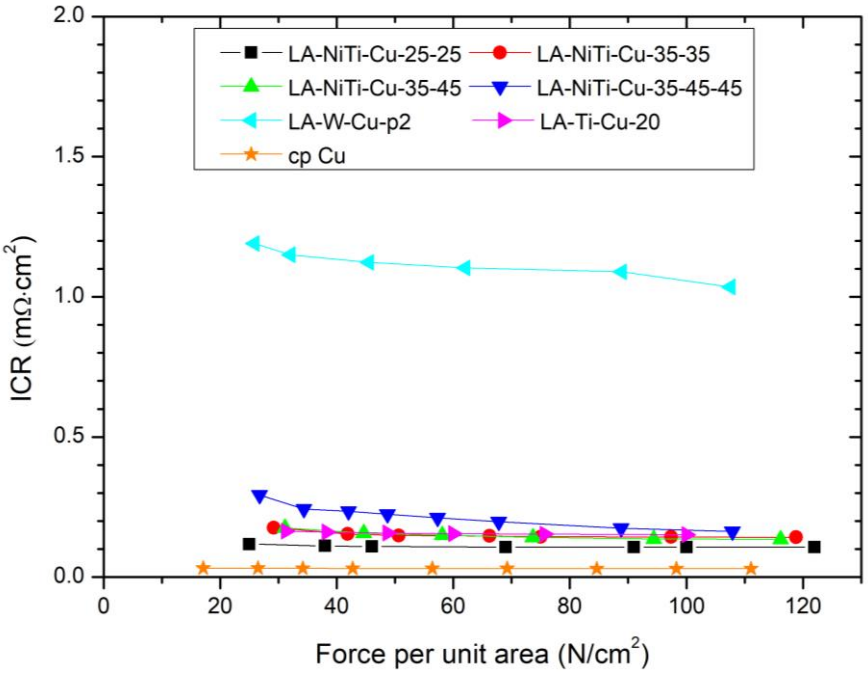

Fig. 16. Plot of ICR versus applied compression force for cp Cu and various samples laser-alloyed with NiTi, W and Ti [y, z].

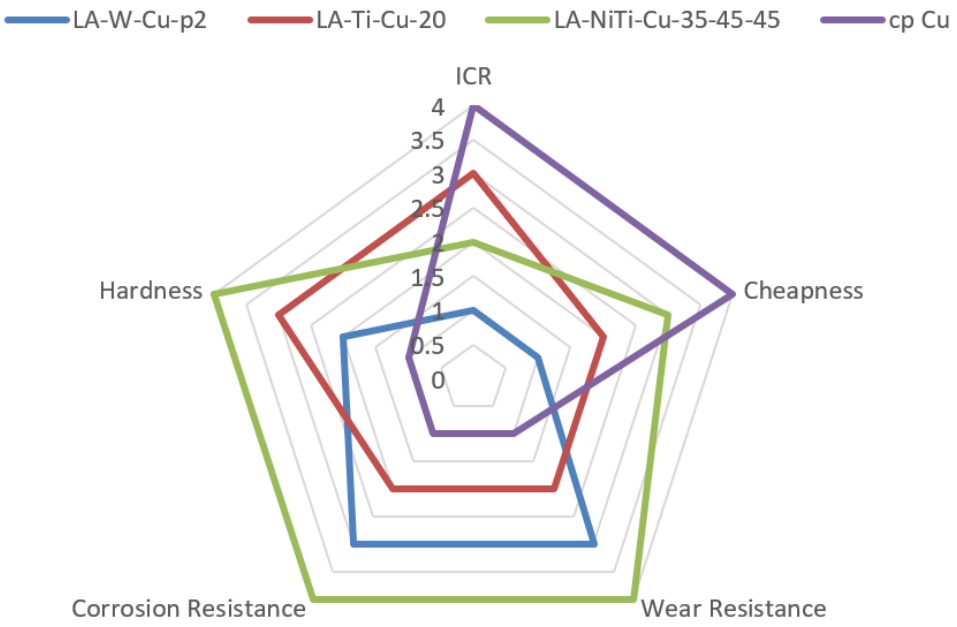

Fig. 17. Radar diagram of various samples.